

Technical Report ARWSB-TR-11011

Evaluation of Flash Bainite in 4130 Steel

G. Vigilante
M. Hespos
S. Bartolucci

JULY 2011



ARMAMENT RESEARCH, DEVELOPMENT AND ENGINEERING CENTER
Weapons & Software Engineering Center
Benét Laboratories



Approved for public release; distribution is unlimited.

The views, opinions, and/or findings contained in this report are those of the author(s) and should not be construed as an official Department of the Army position, policy, or decision, unless so designated by other documentation.

The citation in this report of the names of commercial firms or commercially available products or services does not constitute official endorsement by or approval of the U.S. Government.

Destroy this report when no longer needed by any method that will prevent disclosure of its contents or reconstruction of the document. Do not return to the originator.

REPORT DOCUMENTATION PAGE*Form Approved*
OMB No. 0704-0188

Public reporting burden for this collection of information is estimated to average 1 hour per response, including the time for reviewing instructions, searching data sources, gathering and maintaining the data needed, and completing and reviewing the collection of information. Send comments regarding this burden estimate or any other aspect of this collection of information, including suggestions for reducing this burden to Washington Headquarters Service, Directorate for Information Operations and Reports, 1215 Jefferson Davis Highway, Suite 1204, Arlington, VA 22202-4302, and to the Office of Management and Budget, Paperwork Reduction Project (0704-0188) Washington, DC 20503.

PLEASE DO NOT RETURN YOUR FORM TO THE ABOVE ADDRESS.

1. REPORT DATE (DD-MM-YYYY) JULY 2011	2. REPORT TYPE FINAL	3. DATES COVERED (From - To)
4. TITLE AND SUBTITLE Evaluation of Flash Bainite in 4130 Steel		5a. CONTRACT NUMBER
		5b. GRANT NUMBER
		5c. PROGRAM ELEMENT NUMBER
6. AUTHOR(S) G. Vigilante, M. Hespos, S. Bartolucci		5d. PROJECT NUMBER
		5e. TASK NUMBER
		5f. WORK UNIT NUMBER
7. PERFORMING ORGANIZATION NAME(S) AND ADDRESS(ES) U.S. Army ARDEC Benet Laboratories, RDAR-WSB Watervliet, NY 12189-4000		8. PERFORMING ORGANIZATION REPORT NUMBER ARWSB-TR-11011
9. SPONSORING/MONITORING AGENCY NAME(S) AND ADDRESS(ES) U.S. Army ARDEC Benet Laboratories, RDAR-WSB Watervliet, NY 12189-4000		10. SPONSOR/MONITOR'S ACRONYM(S)
		11. SPONSORING/MONITORING AGENCY REPORT NUMBER
12. DISTRIBUTION AVAILABILITY STATEMENT <p style="text-align: center;">Approved for public release; distribution is unlimited.</p>		
13. SUPPLEMENTARY NOTES		
14. ABSTRACT ARDEC independently evaluated a Flash Bainite process developed by Gary Cola, Jr., Sirius Protection LLC. Chemical analysis, welding (including flash processing after welding), bend, tensile, fracture toughness, x-ray diffraction, impact toughness, and Gleeble heat affected zone tests were performed on AISI 4130 steel plate. When possible, testing was baselined against conventional quench and tempered material. Manufacturability tests demonstrated that Flash Bainite plate is weldable and bendable, and that welded plate can subsequently be flash processed to restore strength. Small tensile residual stresses were measured in the welded plate and approximately two percent retained austenite was measured in the base material. Flash Bainite demonstrated an impressive combination of strength, elongation, ductility and toughness. Moreover, its impact toughness was consistently higher than quench and tempered plate at all test temperatures evaluated. Intergranular cracking was observed on the fracture surface of some the Flash Bainite impact toughness specimens. The impact toughness testing on the Gleeble heat affected zone specimens in the Flash Bainite and quench and tempered conditions exhibited equivalent results. Though this subject testing identified a few issues that need to be addressed, the Flash Bainite processing of 4130 steel demonstrates promise for applications needing a combination of high strength with good elongation, ductility, and toughness (e.g. armor and vehicle). The novel Flash Bainite process for steels has the potential to reduce product cost and weight while also enhancing mechanical performance.		

INSTRUCTIONS FOR COMPLETING SF 298

15. SUBJECT TERMS
Flash Bainite, bainite, bainitic steel, flash processing, 4130 steel

16. SECURITY CLASSIFICATION OF:			17. LIMITATION OF ABSTRACT U	18. NUMBER OF PAGES 45	19a. NAME OF RESPONSIBLE PERSON Greg Vigilante
a. REPORT U/U	b. ABSTRACT U	c. THIS PAGE U			19b. TELEPHONE NUMBER (Include area code) 518 266-5613

--	--

TABLE OF CONTENTS

BACKGROUND	1
EXPERIMENTAL PROCEDURE	2
RESULTS AND DISCUSSION	8
SUMMARY	26
RECOMMENDATIONS	27
ACKNOWLEDGEMENTS	27
REFERENCES	28

LIST OF FIGURES

Figure 1. Schematic of Flash Bainite (FB) process for steel sheet/plate [1]. Copied with permission from G.M. Cola, Jr., Sirius Protection LLC.	1
Figure 2. Conventional plate that was cut longitudinally then welded back together and subsequent FB processed. Note location of bend and tensile specimens welded back together.	3
Figure 3. Location of three residual stress and one retained austenite measurements on top of the plate.	5
Figure 4. Locations of two residual stress measurements on bottom of the plate.	5
Figure 5. Gleeble 1500 at Benét Laboratories used for HAZ simulation testing.	7
Figure 6. Plot of Gleeble HAZ thermal cycle.	7
Figure 7. Typical banding at mid-thickness.	9
Figure 8. Representative FB microstructure.	9
Figure 9. Microhardness of post-weld FB (top) and indent locations in the weldment (bottom). Red boxes indicate banding and possible lack of fusion.	10
Figure 10. Low magnification photo of ER120 weldment (bottom) with microhardness indents labeled (top).	11
Figure 11. Bend specimen before test.	12
Figure 12. Bend specimen after test.	12
Figure 13. Note non-uniformity of the ER120 welds without post-weld heat treatment.	12
Figure 14. Post-weld FB tensile specimens failed at/near the interface of weld metal / base metal.	14
Figure 15. Average CVN impact energy on Flash Bainite vs. Conventional Q&T 4130 steel.	16
Figure 16. Example of cracking near the centerline of specimen FB TL-F5 (from “mill run” plate).	17
Figure 17. Cracking and tearing along the centerline of specimen FB LT-F1 (from “mill run” plate).	17
Figure 18. Fracture surface of Q&T specimen C LT-6.	17
Figure 19. Secondary cracking evident on fracture surface (FB TL-F2, “mill run” plate).	18
Figure 20. Higher magnification image of crack reveals intergranular cracking.	18
Figure 21. Evidence of what appears to be ductile shear lip surrounding the intergranular crack (FB TL-F5, “mill run plate”).	18
Figure 22. Mixed mode fracture (predominantly cleavage) on a Q&T CVN specimen (C LT 10).	18

Figure 23. Low magnification light microscope image of a cross section of specimen FB LT-F1 through region of intergranular cracking. Note that the crack is coincident with the banding in the center of the plate. Etched with 2% Nital.	19
Figure 24. Intergranular secondary cracking in CVN specimen FB LT-F1. Note the concentration of banding where the cracking occurred. MAG 400x.	20
Figure 25. Knoop microhardness indents in etched (2% Nital) CVN specimen FB LT-F1. Note that the indent in the banded region at the top right of the image is smaller (harder) than the indent in the bottom left (softer). MAG 600x.	20
Figure 26. Lightly etched (2% Nital) CVN specimen LT F1. The arrows point to Mn-S inclusions which are preferentially located in lightly banded regions. MAG 1000x.	21
Figure 27. Etched microstructure (2% Nital) of Q&T 4130 plate (CVN C LT 6). The arrow points to a blocky region of ferrite. MAG 1000x.	22
Figure 28. Photomicrographs and microhardness reading across the Gleeble HAZ in FB 4130 plate.	23
Figure 29. Photomicrographs and microhardness readings across the Gleeble HAZ in Q&T 4130 plate.	24
Figure 30. CVN impact toughness after Gleeble HAZ processing. Note the similarity in results between the FB and Q&T 4130 steel.	25
Figures 31. The predominant failure mode of the CVN Gleeble HAZ specimens was brittle cleavage fracture (the above specimen is C TL 04; 3.2J @ -40°C).	25

LIST OF TABLES

Table 1. Chemistry of Flash Bainite 4130 Steel.	8
Table 2. Tensile and Fracture Toughness Summary	13
Table 3. Average CVN impact energy as a function of temperature and orientation.	16

APPENDICES

APPENDIX A Tensile Test Results on “Baseline” FB Plate	30
APPENDIX B Tensile Test Results on Welded, Flattened and FB Plate	31
APPENDIX C Tensile Test Results on FB Plate Welded with ER120 Filler Metal	32
APPENDIX D Representative K_{Ic} Fracture Toughness Result on “Baseline” FB Plate	33
APPENDIX E X-Ray Diffraction Report	34
APPENDIX F Charpy V-Notch Test Results on Flash Bainite and Q&T 4130 Plate	38
APPENDIX G Charpy V-Notch Test Results on Gleeble HAZ Specimens	39

BACKGROUND

In 2010, ARDEC was contacted about Flash Bainite (FB), a rapid manufacturing process which produces a novel steel microstructure with a purported combination of high strength and good elongation and toughness. The process has been demonstrated on plain carbon and lean alloyed steels (e.g. 4130, 8620) ranging from 0.04-0.74 wt. % carbon, and has been performed on a variety of different forms including sheet, plate, and tubing (round and rectangular).

FB processing occurs in less than 10 seconds. Typically, the time above 300°C is less than three seconds. As such, it is an extremely energy efficient and environmentally friendly process. The

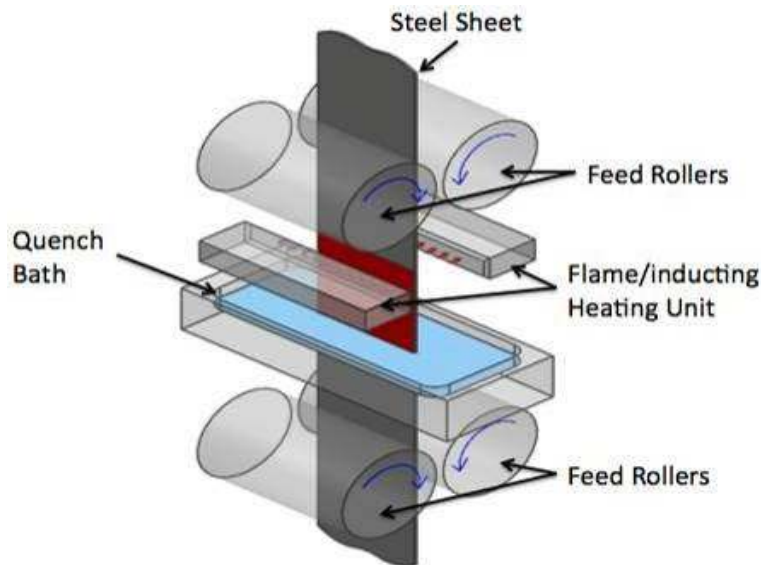


Figure 1. Schematic of Flash Bainite (FB) process for steel sheet/plate [1]. Copied with permission from G.M. Cola, Jr., Sirius Protection LLC.

steel is heated (austenitized) to above 1050°C ($>A_3$) using either oxy-propane or induction heating. After heating, the material is purportedly quenched within milliseconds to near room temperature [1]. Figure 1 shows a schematic of the FB process. Recent improvements have included horizontal processing which enables continuous handling of thicker plates. However, typical plate thicknesses are only 6-9 mm, and the process runs into physical limitations at about 12 mm thickness.

After flash processing, the material is typically tempered at a low temperature (218°C for ~10 min.) to restore some ductility and toughness. The FB processing results in the formation of small, bainitic plates within a matrix of martensite. The rapid heating during processing results in a heterogeneous distribution of carbon within the austenite phase. Upon quenching, the

austenite decomposes to a mixed, composite microstructure with high strength, but also good ductility and toughness [1]. Formations of mixed bainitic/martensitic microstructures have been demonstrated to enhance toughness in 4340 type steels [2, 3]. However, the improvement in toughness was achieved through isothermal processing rather than direct quenching.

After a cursory technology assessment by ARDEC [4], it was determined that the FB process warranted further investigation. This report provides details on the testing performed, determines the applicability of the technology to Army and other applications, and provides recommendations for future testing.

EXPERIMENTAL PROCEDURE

Gary Cola, Sirius Protection LLC, provided 4130 steel plates to ARDEC. Both Benét Laboratories and Picatinny Arsenal received conventional steel plates (spheroidized condition, not heat treated) and FB processed plates. Typically, Sirius Protection LLC has flash processed “mill run” plate rather than spheroidized plates. All plates came from the same lot of 4130 steel. Each plate was nominally 305 mm wide x 610 mm long by 6.35 mm thick (12 in. foot wide by 24 in. long by 0.25 in. thick).

The FB plates received by Picatinny Arsenal were crack free, whereas some macroscopic quench cracks were observed in the plate received by Benét Laboratories. The cracks were in the transverse orientation at the edges of the plate. Due to the severe quench experienced by the plate during the flash processing, it was not surprising that cracking occurred. In response to the quench cracking, Sirius Protection LLC provided an additional FB plate to Benét Laboratories for testing. This plate was from the more commonly used “mill run” condition (normalized to produce a mixture of ferrite and pearlite) versus the spheroidized plate (spheroids of cementite uniformly distributed in a matrix of ferrite) previously provided.

In order to characterize FB, the following tests were performed:

Chemical Analysis

Chemistry of the as-received FB plates was determined by arc spark spectroscopy. Carbon and sulfur contents were measured by the combustion, infrared absorption method in accordance with ASTM E1019.

Welding

A single conventional plate and a single FB plate were cut lengthwise and welded back together using a butt weld (Figure 2). To determine the effects of post-weld heat treatment, the conventional 4130 plate was welded with 4130 filler metal. When restraints were removed, significant distortion was noted. To flatten, the plate was sandwiched between two heavy plates in an oven at 760°C (1400°F). Then, the welded and flattened plate underwent the FB process. For comparison to a shorter process, the FB plate was welded with ER120 filler.

Plates were preheated to 93°C (200°F). Pulsed gas-metal arc welding was performed with a Lincoln Power Wave 455 power supply. The butt joint had a 60-degree groove and 1.6mm (0.062 in.) root opening. A fixture was used to contain the 100% argon backing gas. Two passes

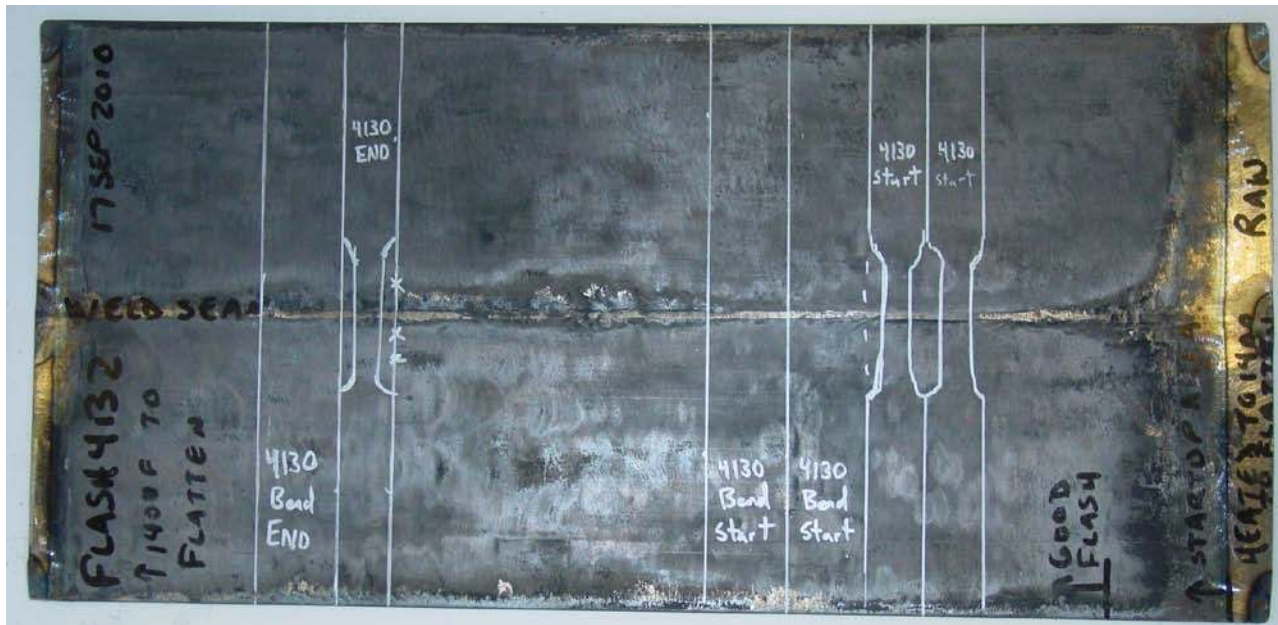


Figure 2. Conventional plate that was cut longitudinally then welded back together and subsequent FB processed. Note location of bend and tensile specimens welded back together.

filled the groove. The 1.1mm (0.045 in.) diameter 4130 wire did not flow well. Both plates were welded with same parameters (except wire composition as noted above).

Metallographic specimens were taken across the joint to include weld metal, heat-affected zone (HAZ) and base metal. Specimens were mounted, ground and polished to observe the unetched and etched microstructure. Microhardness testing was conducted on metallography

specimens in accordance with ASTM E384 (Diamond Pyramid Hardness (DPH) or Vickers (HV) with 1000-gram load). Then, specimens were etched with 2% Nital.

Bend Testing

Bend testing is one measure of manufacturability. Bend testing was performed on welded FB with both the 4130 and ER120 filler metals. Figure 2 shows the bend specimen location and orientation. Bend specimens were ground to 3.2mm thickness (0.125 in.) and corners were radiused to avoid stress risers. A 102mm (4.0 in.) diameter mandrel gave a theoretical elongation of ~3% on the outermost bend fibers.

Tensile Testing

Ten rectangular, 50mm gage length tensile specimens were machined and tested in accordance with ASTM E8. Three “baseline” tensile specimens, from FB treatment, were oriented longitudinally, i.e. along the rolling direction. For the welded plates, see Figure 2 for the tensile specimen location and orientation. Hardness was tested in accordance with ASTM E18 on tensile specimen grips using the Rockwell C scale (HRC). Prior to measuring, the specimens were lightly etched to reveal weld location.

Fracture Toughness Testing

Three (3), three-point bend fracture toughness specimens (B, thickness = 6.35mm) were electro-discharged machined, ground and tested in accordance with ASTM E399 at room temperature. The fracture toughness specimens were oriented in the T-L direction so that the crack propagated parallel to the rolling direction.

XRD Testing

A cursory x-ray diffraction measurement was intended to ascertain minimal retained austenite in 4130 base metal after FB heat treatment. Welding created distortion, so residual stress was also measured. X-ray diffraction measurements were outsourced to American Stress Technologies. Their techniques complied with SAE 784a, ASTM E915 and ASTM E975.

Five residual stress measurements were taken in and around the ER120 joint to characterize the stress distribution around the weld. Figure 3 shows locations of three residual stress and one retained austenite measurements on top of the plate, and Figure 4 shows location of two

residual stress measurements on bottom of the plate. A 6th residual stress measurement (not shown) was taken away from the weld on bottom of the plate.



Figure 3. Location of three residual stress and one retained austenite measurements on top of the plate.



Figure 4. Locations of two residual stress measurements on bottom of the plate.

Charpy V Notch Testing

Charpy V Notch (CVN) impact testing was performed on 4130 plate in accordance with ASTM E23. The following material processing conditions were evaluated:

- As-received Flash Bainite (from spheroidized plate)
- As-received Flash Bainite (from “mill run” plate)
- Quench and Tempered (Q&T; spheroidized plate)
- Gleeble Heat Affected Zone (HAZ) processed - Flash Bainite (spheroidized plate)
- Gleeble HAZ processed - Q&T (spheroidized plate)

The Q&T condition was produced by austenitizing the as-received spheroidized plate at 830°C for approximately 20 minutes (at temperature), oil quenching, and tempering at approximately 190°C for at least 20 minutes (at temperature). This heat treatment resulted in a hardness

range of approximately HRC 47-52 for the Q&T material versus approximately HRC 46-50 for the FB material. Hardness readings were taken on the plate material before specimen fabrication.

Subsize, 5 mm wide specimens (as per ASTM E23-07a Figure A3.1) were fabricated from the 6.35 mm thick plate. Specimens were taken in both the longitudinal and transverse orientations, henceforth referred to as L-T and T-L, respectively. All specimens from spheroidized plate were tested at 20°C, 5°C, -10°C, -25°C, and -40°C. The FB from the “mill run” plate was only tested at 20°C and -40°C. All conditions were tested in triplicate. After testing, fractography and metallography were performed on select specimens.

Gleeble Heat Affected Zone (HAZ) Simulation Testing

Gleeble heat affected zone (HAZ) testing was performed on both FB and conventional Q&T 4130 plate (both from same lot of spheroidized plate) using blanks (60mm x 10mm x 5mm) taken from the longitudinal and transverse orientations. The Gleeble is a thermo-mechanical, servo-hydraulic testing machine that was developed for weld simulation and workability testing of conductive materials, such as steels. Use of resistance heating enables heating rates as high as 10,000°C/s. Figure 5 shows a picture of a Gleeble 1500 at Benét Laboratories.

For the Gleeble HAZ testing, a Hannerz thermal cycle program was used. Inputs included a 1MJ/m heat input, a peak temperature of 1100°C, a cooling time from 800-500°C in 10 seconds ($\Delta t_{800/500}$), and a total processing time of 200s. The $\Delta t_{800/500}$ cooling time was ascertained based on empirical relationship for cooling rate [5]. Figure 6 shows the temperature vs. time profile for the Gleeble HAZ thermal cycle.

Subsize Charpy V-Notch specimens were subsequently fabricated (as per ASTM E23-07a Figure A3.1) from the Gleeble HAZ blanks and tested in the same manner as described previously (in triplicate in two orientations and five different test temperatures) in order to determine how the thermal cycle affected impact toughness. The notch was taken in the center of the HAZ.



Figure 5. Gleeble 1500 at Benét Laboratories used for HAZ simulation testing.

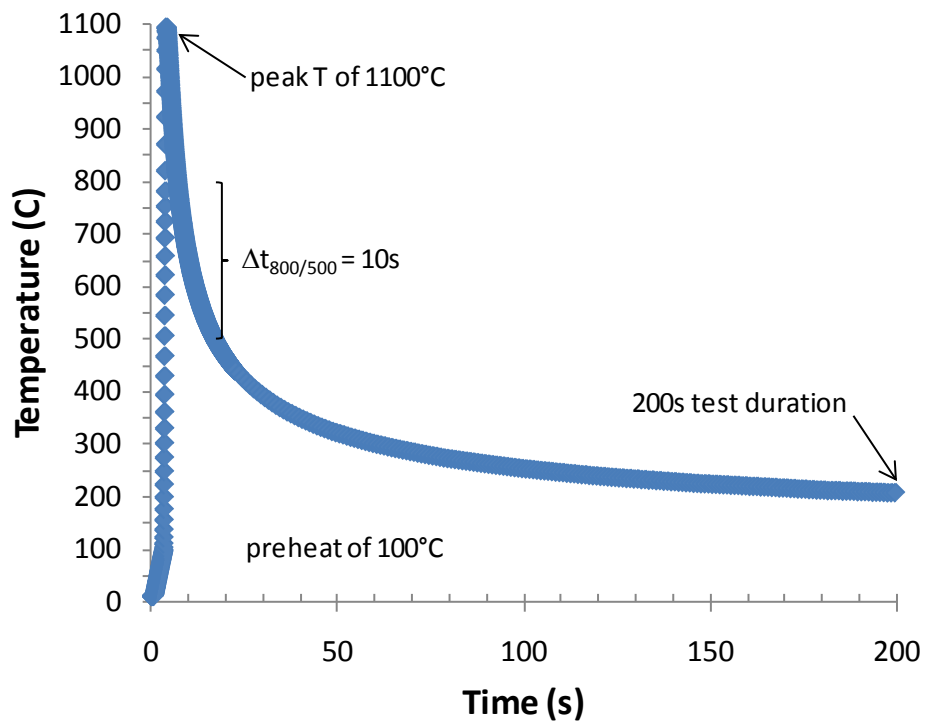


Figure 6. Plot of Gleeble HAZ thermal cycle.

RESULTS AND DISCUSSION

Chemical Analysis

The chemical analysis, shown in Table I below, complies with specified limits for 4130 steel. The phosphorus level is within specification limit, but improved toughness may be achieved by maintaining minimal phosphorus content (i.e. – less than 0.010%). Sulfur for this current lot, 0.002%, is quite low. The elements on right-hand side of table have no individual specification limits.

Table 1. Chemistry of Flash Bainite 4130 Steel.

<u>Element</u>	<u>Actual</u>	<u>Specified</u>		<u>Element</u>	<u>Actual</u>
C	0.3	0.28 - 0.33		V	0.002
Si	0.203	0.2 - 0.35		W	0.004
S	0.002	0.04 max		Ti	0.005
P	0.011	0.04 max		As	0.005
Mn	0.534	0.40 - 0.60		Sn	0.011
Ni	0.056	0.25 max		Co	0.005
Cr	0.917	0.8 - 1.10		Al	0.027
Mo	0.166	0.15 - 0.25		Pb	0.002
Cu	0.128	0.35 max			

Welding

Banding was prevalent at mid-thickness of “baseline” FB material (Figure 7). Banding, which is common in steel, was observed in all specimens. It is usually attributed to chemical segregation. A brief literature search finds that reducing the banding by thermomechanical treatment might not be practical (economically), and that reducing the banding might not improve mechanical properties. Conversely, at these high strength levels, 4130 is sensitive to inhomogeneities and reducing the banding may improve properties. This merits additional evaluation [6].

Figure 8 shows typical FB microstructure. The red box highlights a possible micro-crack. Photo confirms previous work that FB produces a microstructure consisting of approximately 20% bainite and 80% martensite [7].

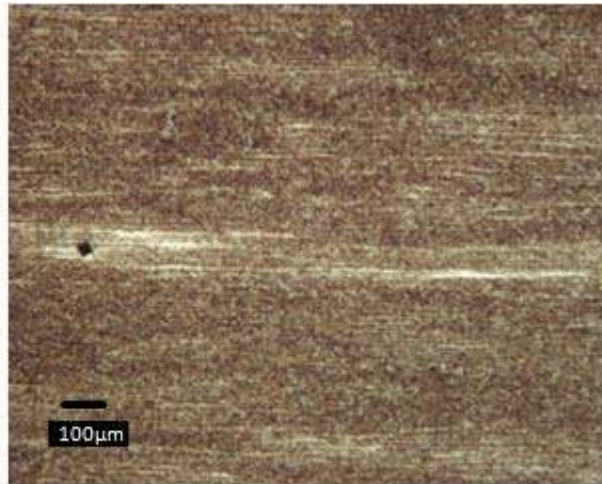


Figure 7. Typical banding at mid-thickness.

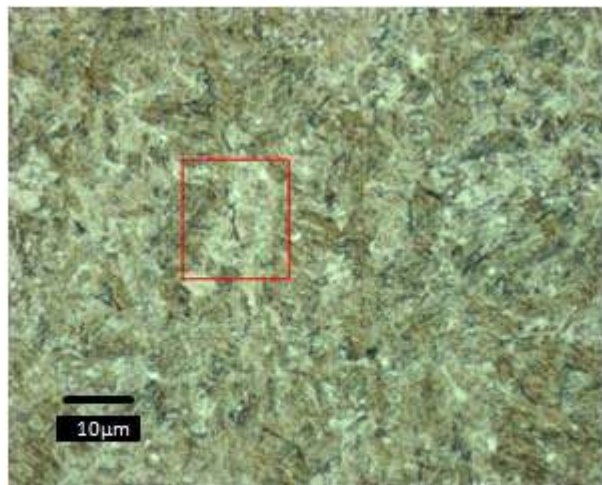


Figure 8. Representative FB microstructure. The red box indicates possible micro-crack. n
possible lack of penetration at root of weld (Figure 9). Ignore the decarburization layer from flattening. The microhardness indents numbered in bottom image correlate to the microhardness indent number in the chart.

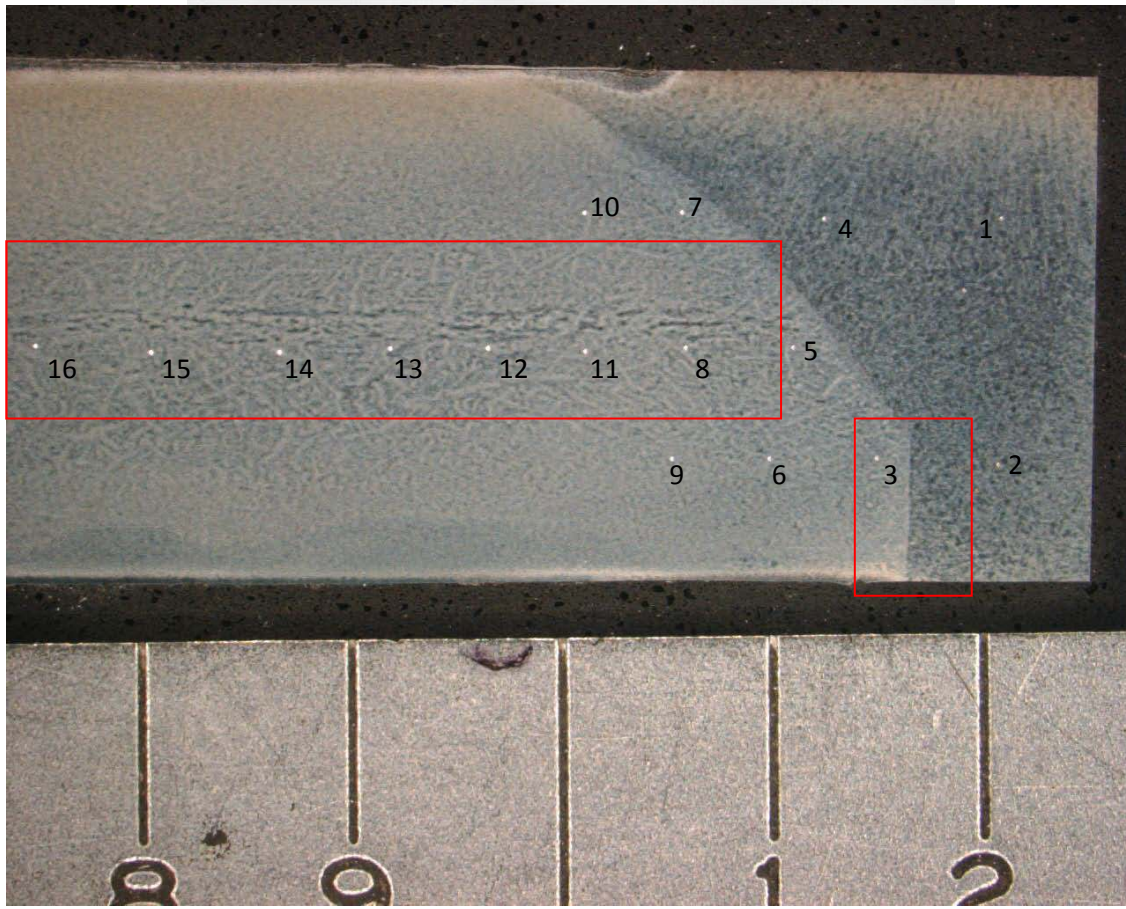
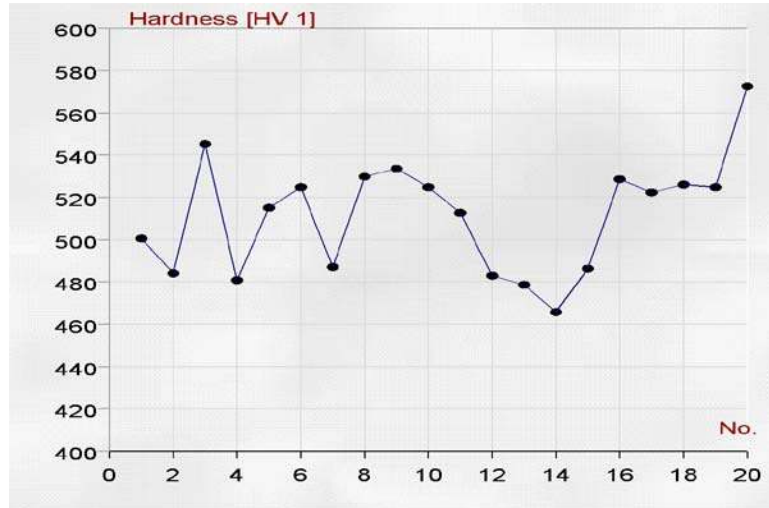


Figure 9. Microhardness of post-weld FB (top) and indent locations in the weldment (bottom). Red boxes indicate banding and possible lack of fusion.

Figure 10 (bottom) is a low magnification photo of ER120 weldment with microhardness indents labeled. Note the two-pass weld and HAZ. As expected, the ER120 has a weak link in weld metal and HAZ. Note that away from the weld (indents #19 & 20 not in photo), in a banded area, a microhardness of HV634 was measured.

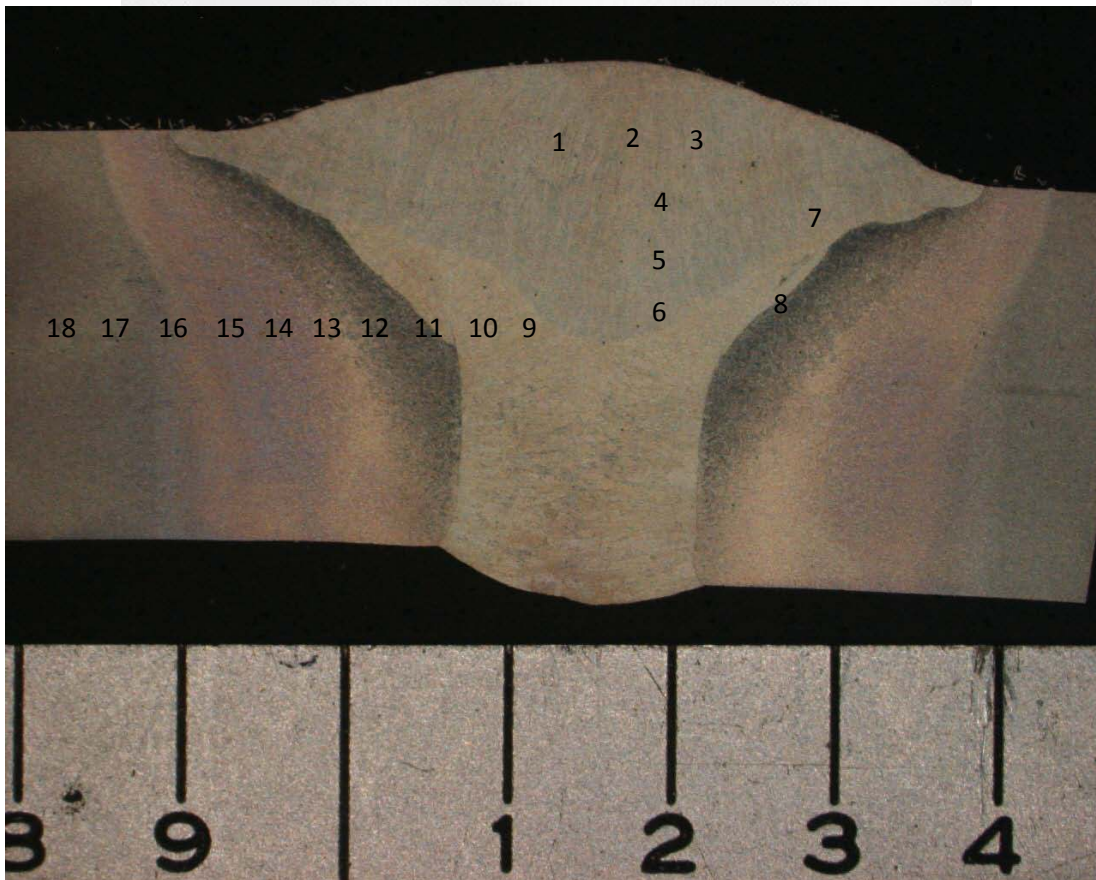
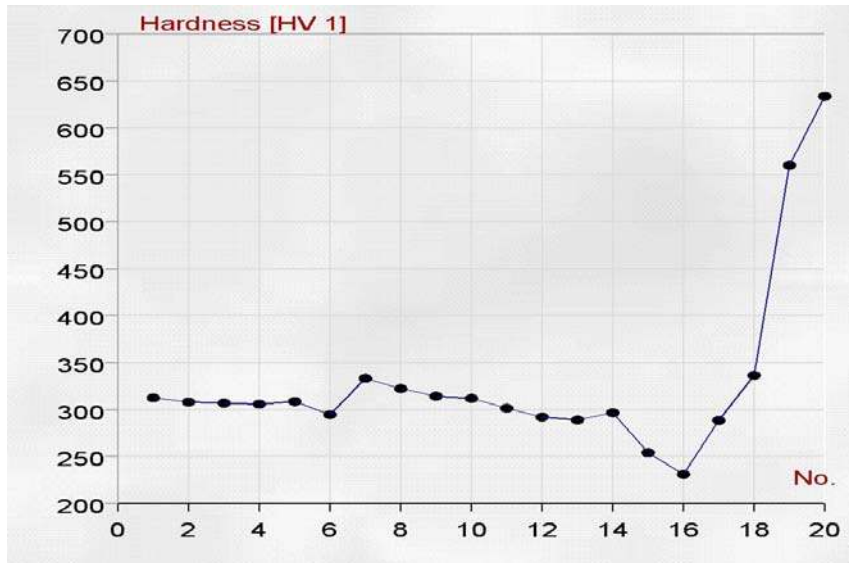


Figure 10. Low magnification photo of ER120 weldment (bottom) with microhardness indents labeled (top).

Bend Testing

Figures 11 and 12 show a welded specimen before and after the bend test. All specimens passed the bend test; however, there is significant non-uniformity of the ER120 welds without post-weld heat treatment (see Figure 13, specimen DE1). The ER120 HAZ is the weak link. The post-weld FB specimen, shown as “DD1” in Figure 13, bent uniformly. Prior to testing, there were no visual weld defects on any specimens.



Figure 11 (left). Bend specimen before test.



Figure 12 (right). Bend specimen after test.

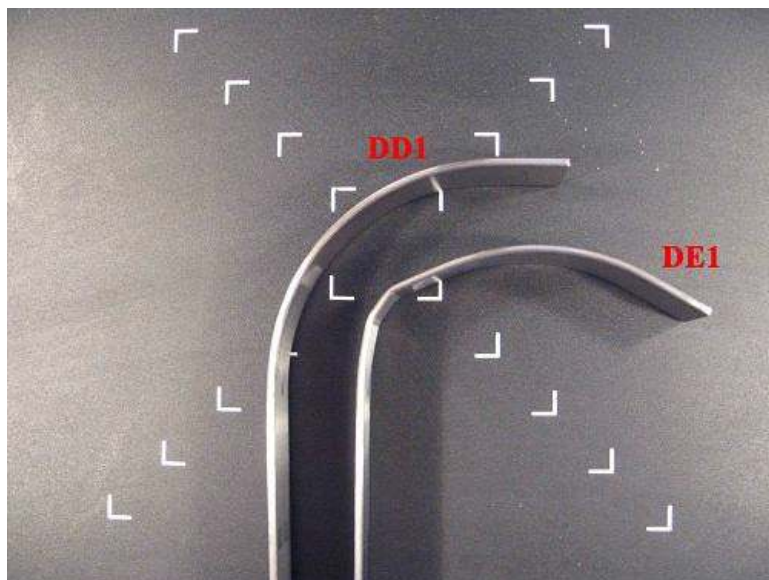


Figure 13. Note non-uniformity of the ER120 welds without post-weld heat treatment.

Tensile and Fracture Toughness Testing

Table 2 summarizes tensile and fracture toughness testing. Note the impressive properties of the as-received FB. The average of three consistent tests is shown. K_{Ic} results passed all validity checks.

Welding with 4130 wire followed by FB post-weld heat treatment produces the same yield strength as unwelded FB; however, at least half of the ductility is lost in the welded area. A welding engineer observed lack of penetration, which might have contributed to loss of ductility. That is, there appears to be a lack of penetration at weld root. These post-weld heat treated tensile specimens failed at or near the interface of weld metal / base metal (Figure 14).

FB followed by welding with ER120 filler has about half the strength of post-weld heat treated FB. All four specimens failed in heat affected zone about 3 mm away from weld metal. There was a double neck on other side of HAZ about 3 mm from weld metal. Specimen failure occurred in area of mixed transformation products. Refer to Appendices A-D for detailed tensile and fracture toughness results.

Table 2. Tensile and Fracture Toughness Summary

<u>Condition</u>	<u>Yield Strength (MPa)</u>	<u>Peak Strength (MPa)</u>	<u>% Elong'n</u>	<u>Max % Strain</u>	<u>% Redux'n in Area</u>	<u>K_{Ic} (MPa sqrt(m))</u>
As-received FB	1469	1834	14.5	14.4	37	66
Weld w/4130 Wire, then FB	1455	1758	5.9	4.9	15	Not measured
FB, then Weld w/ER120 Wire	738	889	5	4.4	31	Not measured
<u>Condition</u>	<u>(KSI)</u>	<u>(KSI)</u>				<u>K_{Ic} (KSI sqrt(in))</u>
As-received FB	213	266	14.5	14.4	37	60
Weld w/4130 Wire, then FB	211	255	5.9	4.9	15	Not measured
FB, then Weld w/ER120 Wire	107	129	5	4.4	31	Not measured

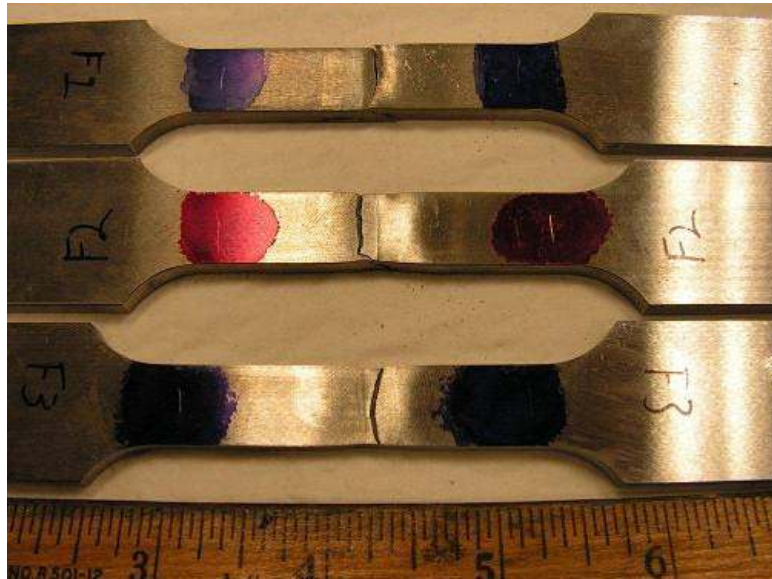


Figure 14. Post-weld FB tensile specimens failed at/near the interface of weld metal / base metal.

XRD Testing

When compared to the 1468 MPa (213 KSI) tensile yield strength, the magnitude of residual stresses is relatively low: about 220 MPa (32 KSI). However, most of the residual stresses measured are tensile, not compressive. Importantly, the tensile residual stresses create susceptibility to embrittling mechanisms, such as stress corrosion. And, the maximum residual stresses were detected in two areas: on the weld and on the bottom of the plate away from weld. The typical residual stress distribution around the weld was not detected perhaps because it does not exist, or it relieved when sectioned, or it was not measured (need to test more areas).

Appendix E contains details of x-ray diffraction testing, including “changes in peak width (FWHM) relative to location.” Peak width from top of plate is narrower than from bottom of plate indicating a grain size or other difference between top and bottom. Wider peak indicates residual cold work, finer particle size, or, in the case of quench and tempered steel, micro-strain from transformation [8]. However, both microhardness and microstructure were consistent from the top to bottom of the plate thickness.

Approximately 2% retained austenite was measured via XRD testing. This is consistent for 4130 in which an aggressive quench is utilized.

Charpy V-Notch Testing

The averaged results on the CVN testing can be found in Table 3 and Figure 15. For the complete CVN results, please see Appendix F. Note that the average FB data from the “mill run” plate are shown as separate data. The FB impact energy at all temperatures was consistently and significantly higher than the conventional, Q&T specimens. Because these are subsize specimens, the energy absorbed cannot be compared to full size specimens. The correlation in impact energy from one-half size to full size specimens is approximately 1.5x [9, 10]. Therefore, for this subsize geometry used, an impact energy of 10 J roughly corresponds to 15 J for a full-size specimen.

Hardness readings on select CVN specimens after testing revealed that the FB specimens were approximately HRC 52-53 while the Q&T specimens were approximately HRC 46-47. This differs from the hardness readings taken on the as-received and heat treated plates. The discrepancy could be due to the surface condition of the plate (e.g. oxide etc.) and any warping of the plate. A hardness of HRC 46-47 likely corresponds to a microstructure which is at least 75% martensite [11].

After CVN testing, specimens from each material condition, orientation, and test temperature were evaluated using light microscopy and Scanning Electron Microscopy (SEM). Of the 14 FB specimens subsequently evaluated, seven contained clear evidence of intergranular cracking in “veins” along the center 20-25% of the specimen. All (4) FB specimens from the “mill run” plate and three of ten FB specimens from the spheroidized plate exhibited intergranular cracking near the centerline. *None of the Q&T specimens examined exhibited any evidence of intergranular cracking.* Figures 16 and 17 clearly show evidence of cracking and tearing along the centerline of (2) FB specimens from “mill run” plate. Contrast that with Figure 18 in which no secondary cracking/tearing is observed (Q&T plate). Figures 19 and 20 are SEM fractographic images of the same FB specimen. In the higher magnification image (Figure 20), intergranular cracking is evident. In many cases in which intergranular cracking was observed, the region surrounding the cracking was ductile and exhibited features which appeared to be shear lips (e.g. Figure 21). All intergranular facets appeared clean and free from an oxide. This was confirmed by Energy Dispersive Spectroscopy (EDS). Therefore, the occurrence of intergranular cracking is believed to be due to the material condition rather than a quench crack during processing. This is more evident after metallographic examination, discussed next. The Q&T specimens exhibited a mixed mode (predominantly cleavage) fracture. Figure 22 is a representative image from a Q&T specimen after CVN testing.

Table 3. Average CVN impact energy as a function of temperature and orientation.

Flash Bainite		
Temp (°C)	Orientation	Ave. Impact Energy (J)
-40	L-T	8.1
-25		7.7
-10		10.0
5		10.4
20		11.5
-40	T-L	10.4
-25		7.9
-10		10.8
5		11.7
20		15.2

Conventional Q&T		
Temp (°C)	Orientation	Ave. Impact Energy (J)
-40	L-T	3.0
-25		3.5
-10		5.4
5		5.6
20		5.8
-40	T-L	3.2
-25		3.3
-10		3.9
5		3.6
20		5.4

Flash Bainite - Mill Run		
Temp (°C)	Orientation	Ave. Impact Energy (J)
-40	L-T	6.7
20		15.6
-40	T-L	6.1
20		11.1

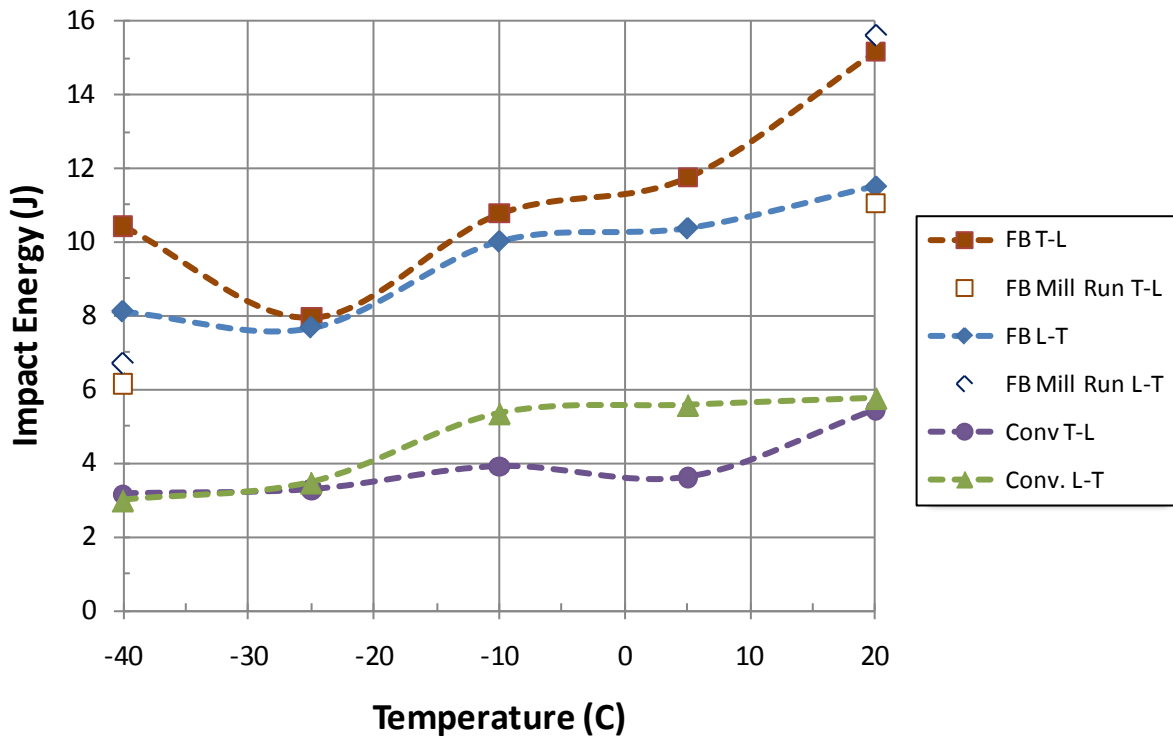


Figure 15. Average CVN impact energy on Flash Bainite vs. Conventional Q&T 4130 steel.

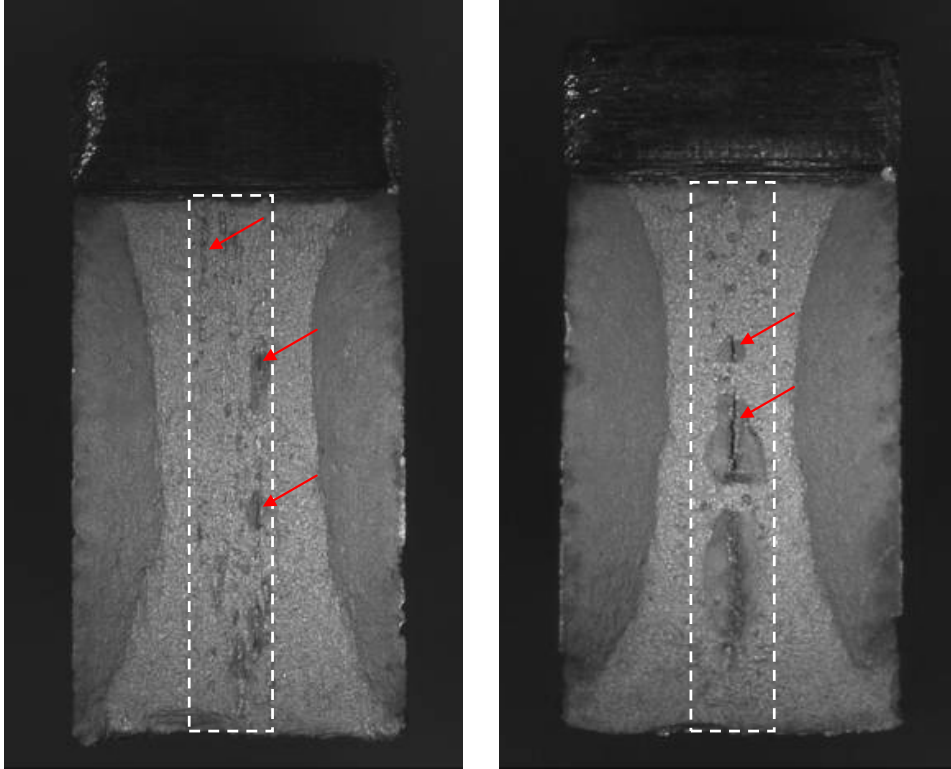


Figure 16 (Left). Example of cracking near the centerline of specimen FB TL-F5 (from “mill run” plate).

Figure 17 (Right). Cracking and tearing along the centerline of specimen FB LT-F1 (from “mill run” plate).

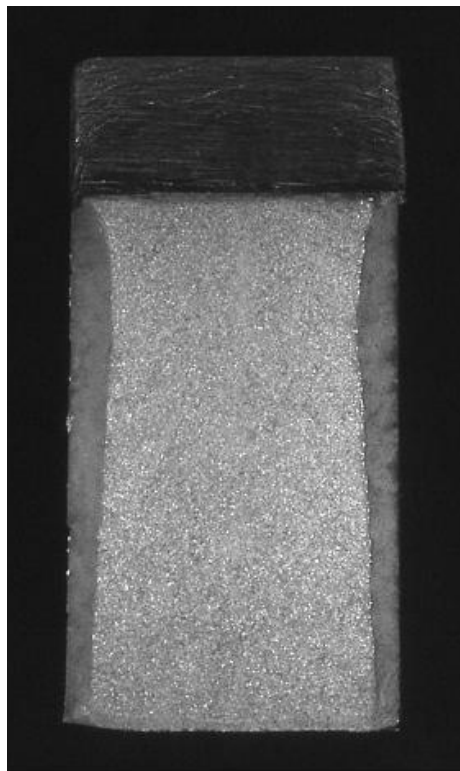


Figure 18. Fracture surface of Q&T specimen C LT-6.

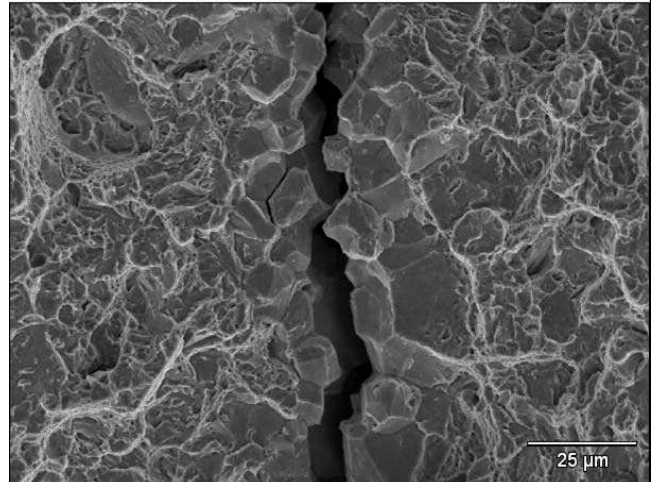
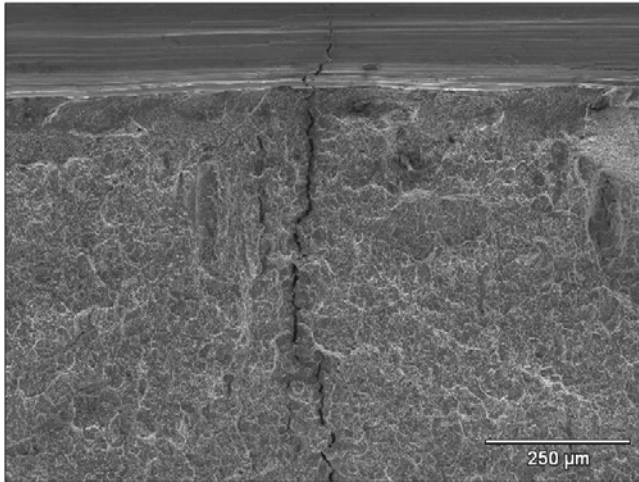


Figure 19 (Left). Secondary cracking evident on fracture surface (FB TL-F2, “mill run” plate).

Figure 20 (Right). Higher magnification image of crack reveals intergranular cracking.

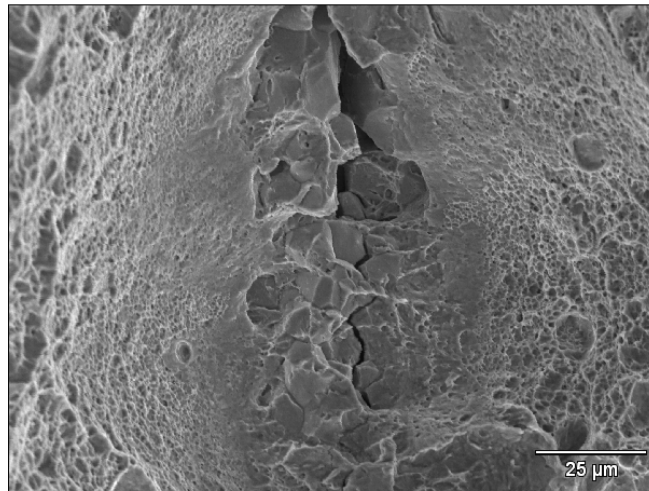


Figure 21. Evidence of what appears to be ductile shear lip surrounding the intergranular crack (FB TL-F5, “mill run plate”).

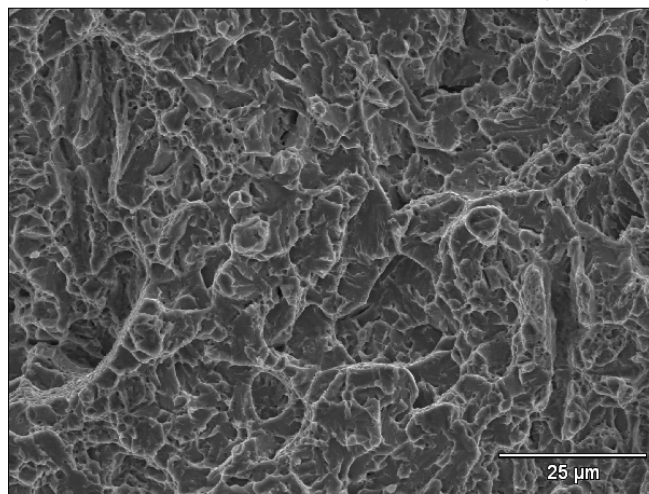


Figure 22. Mixed mode fracture (predominantly cleavage) on a Q&T CVN specimen (C LT 10).

After CVN testing, select specimens were cross-sectioned and metallographically prepared. After etching with a 2% Nital solution, banding was evident. While banding was present on all of the metallographic specimens examined, it was most evident and extreme in a specimen from “mill run” plate. Figure 23 shows a low magnification image of the cross section of CVN specimen FB LT-F1 (from “mill run” plate). A large band is clearly evident along the centerline of the specimen. Intergranular cracking was coincident with the banded region in the center of the specimen. This banding is a result of chemical segregation during the steel making process. It is plausible that the banding was more severe on the “mill run” plate because that microstructure (pearlite and ferrite) is more heterogeneous than a spheroidized microstructure. Figure 24 shows a magnified view of Figure 23 in which the intergranular secondary cracking is clearly evident.

Knoop microhardness readings taken on specimen FB LT-F1 clearly demonstrated that the lightly banded regions were considerably harder than the dark banded regions. This is evident in Figure 25 in which the indent in the upper right of the image (in the light band) is smaller than the indent in the lower left of the image (in a dark band). Note in Figure 25 that the Knoop microhardness indents are not symmetric. This could be due a perpendicularity issue or an indenter alignment issue. However, the conclusion (hardness difference) remains the same. The hardest microhardness reading taken was $HK_{1000}920$ at the center of the specimen in a light band. As per ASTM E140, this corresponds to HRC 68, considerably higher than the maximum hardness (macro) that is attained with 4130 steel. However, heterogeneous chemical segregation could certainly account for the locally high microhardness (and could influence the

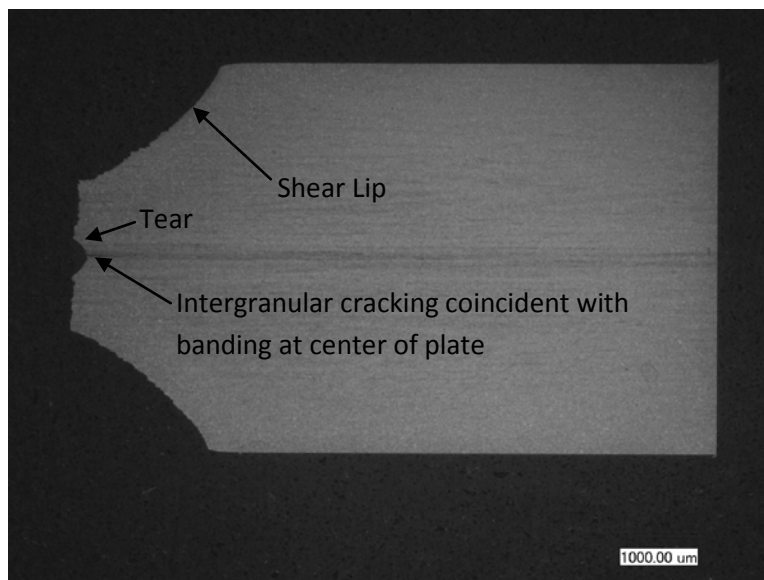


Figure 23. Low magnification light microscope image of a cross section of specimen FB LT-F1 through region of intergranular cracking. Note that the crack is coincident with the banding in the center of the plate. Etched with 2% Nital.

kinetics of tempering). Additionally, Mn-S inclusions appeared to be preferentially located along the lightly banded regions near the center of the specimen (Figure 26). Though the sulfur (S) and phosphorous (P) measured in the chemical analysis are well within the limits for 4130 steel, their presence in the microstructure (as Fe-S and Fe₃P) are well known in causing embrittlement of steels [12]. Segregation of these tramp elements to the centerline of the plate during steel making would only exacerbate the tendency for embrittlement.

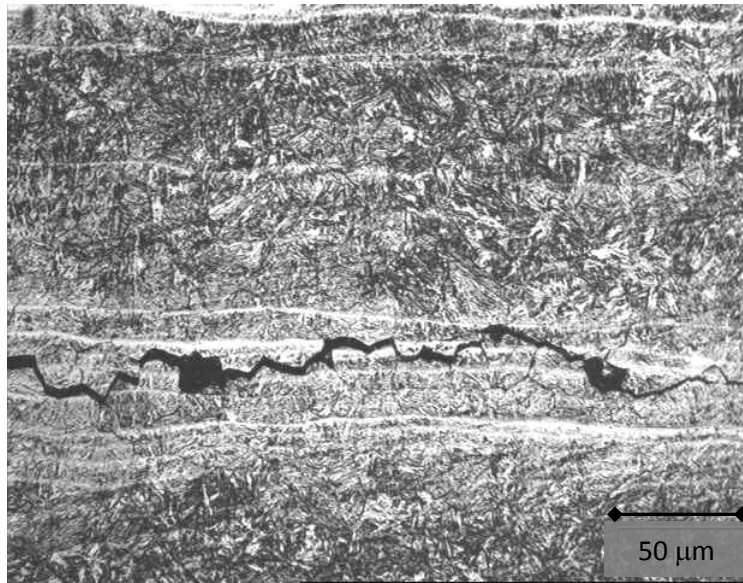


Figure 24. Intergranular secondary cracking in CVN specimen FB LT-F1. Note the concentration of banding where the cracking occurred. MAG 400x.

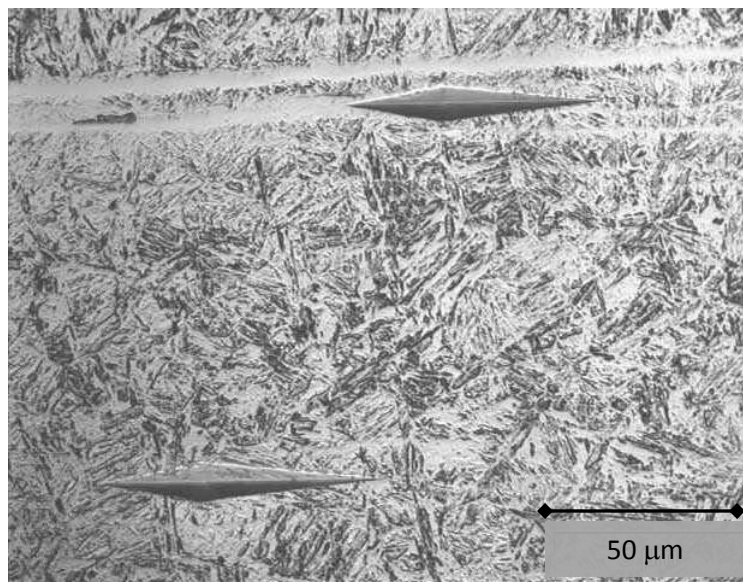


Figure 25. Knoop microhardness indents in etched (2% Nital) CVN specimen FB LT-F1. Note that the indent in the banded region at the top right of the image is smaller (harder) than the indent in the bottom left (softer). MAG 600x.

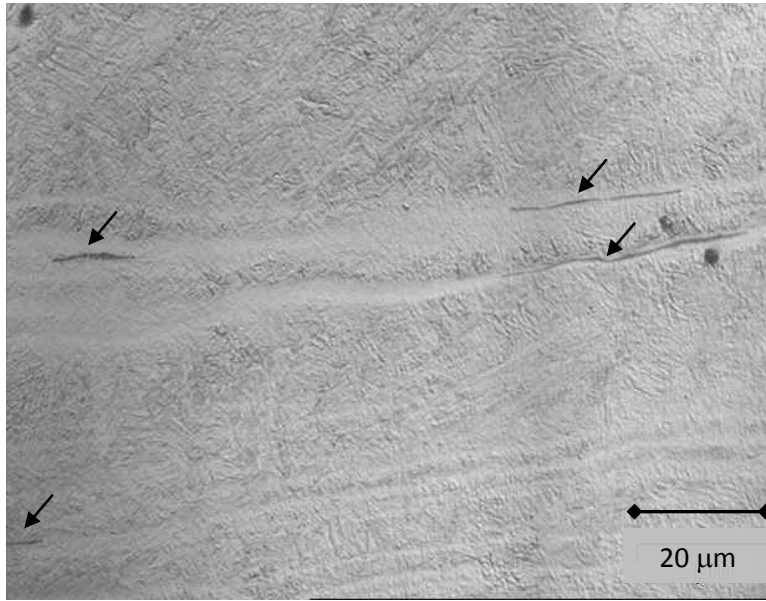


Figure 26. Lightly etched (2% Nital) CVN specimen LT F1. The arrows point to Mn-S inclusions which are preferentially located in lightly banded regions. MAG 1000x.

The appearance of light banded regions with extremely high microhardness suggests the presence of untempered martensite caused the intergranular cracking that was observed after CVN testing. The reasons that the cracking occurred near the centerline of the specimens are because: 1) that is where the chemical segregation is most severe in plate stock, and 2) because the temper was insufficient to convert the hard and brittle untempered martensite to more ductile and tough tempered martensite. Any issues with chemical segregation are likely worse with the “mill run” plate than with the spheroidized plate because of microstructural differences and distribution of carbon. According to Sirius Protection LLC, the FB plates were tempered for a *total* furnace time of 10-11 minutes at 218°C. This time is believed to be insufficient to effectively temper the entire plate resulting in a higher tendency for centerline cracking.

Krauss states that low temperature tempered (LTT) steels such as the subject FB steels are “highly susceptible to brittle intergranular failure caused by quench embrittlement” [13]. Quench embrittlement should not be confused with quench cracking or temper embrittlement. Quench embrittlement typically occurs in steels have greater than 0.5 wt. % C but can also occur in lower carbon steel which have high P. Additionally, use of lower austenitizing temperatures retains carbides (lower the amount of C in the austenite) and reduces the sensitivity of intergranular fracture in LTT steels. In FB processing, the austenitizing temperature is high (>1050°C), but the time at temperature is only a few seconds. There is also a tradeoff to manage between austenitizing temperature and mechanical properties. A higher

austenitizing temperature tends to increase fracture toughness, while a lower austenitizing temperature tends to increase impact energy, % elongation, and % reduction in area [14-16].

Interestingly, the region surrounding many of the intergranular cracks and tears in the CVN specimens contained what appeared to be shear lips, an indicator of ductility (e.g. Figure 21). Moreover, the intergranular cracking occurred normal to the primary crack plane. This off-axis cracking could actually be beneficial as it would increase the amount of energy absorbed.

Figure 27 shows the microstructure of a Q&T CVN specimen. The microstructure is predominantly martensite with other austenite decomposition products such as bainite and some blocky ferrite (arrow).

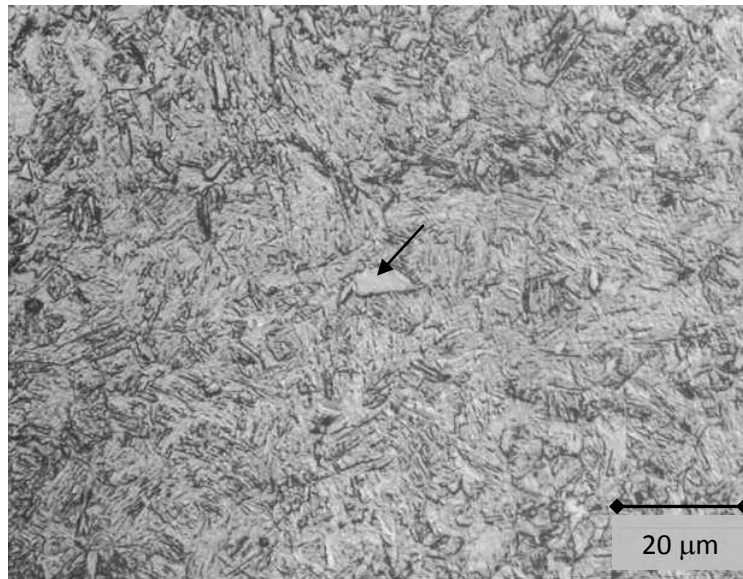


Figure 27. Etched microstructure (2% Nital) of Q&T 4130 plate (CVN C LT 6). The arrow points to a blocky region of ferrite. MAG 1000x.

Gleeble Heat Affected Zone (HAZ) Simulation Testing

Based on the thermal profile in Figure 6, the Gleeble HAZ processing raised the temperature of the blanks into the austenite region (1100°C) followed by cooling to the martensite start temperature (~350°C) over approximately 35 seconds. A microhardness traverse was taken across the Gleeble HAZ region. The results can be found in Figures 28 and 29. The HAZ processing on the FB plate and Q&T plate resulted in a mixed microstructure with a microhardness of HV₅₀₀331-417 and HV₅₀₀330-361, respectively. The subsequent CVN specimens were fabricated from the blanks with the notch in the center of the specimen (center of the HAZ).

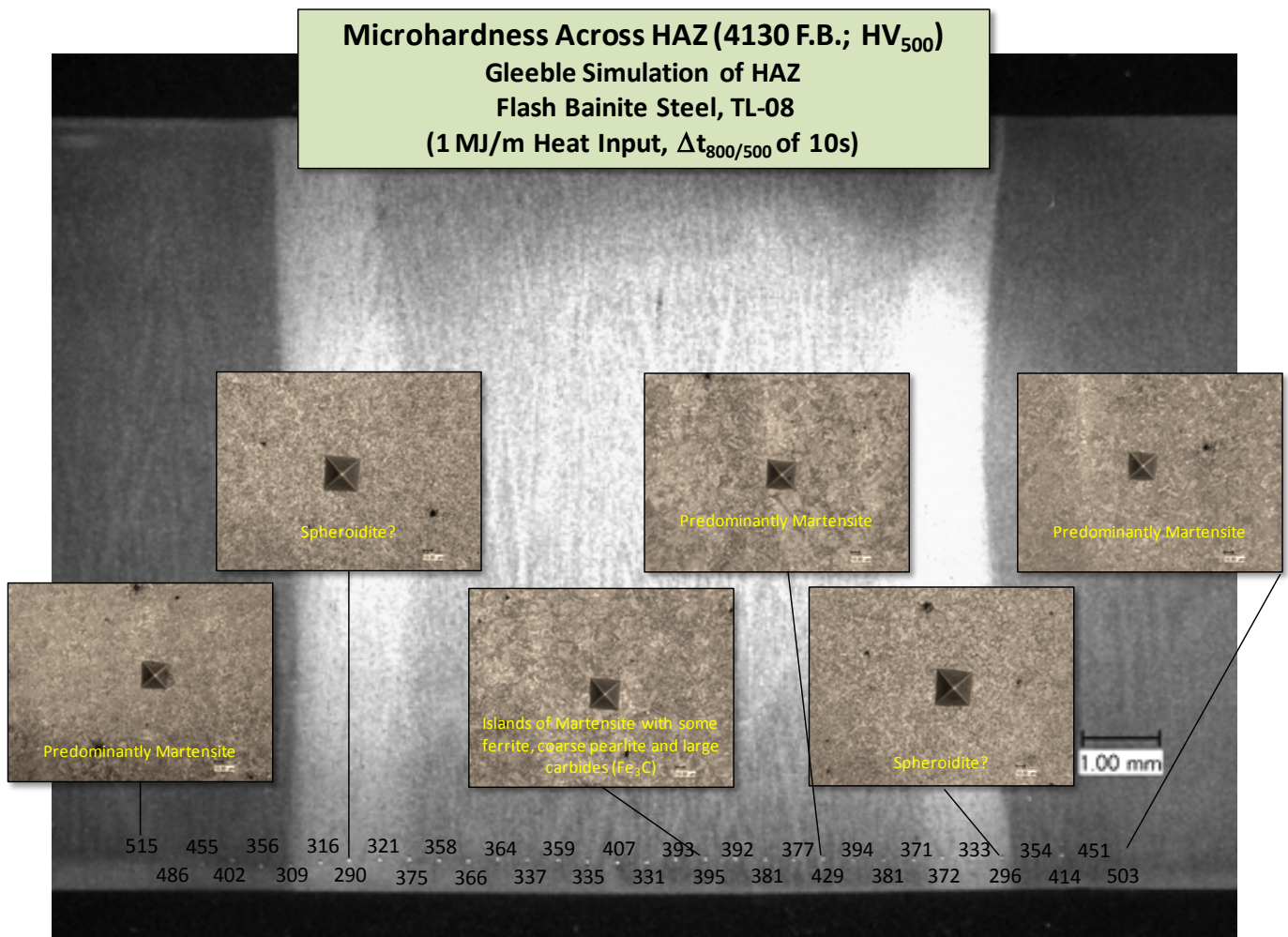


Figure 28. Photomicrographs and microhardness reading across the Gleeble HAZ in FB 4130 plate.

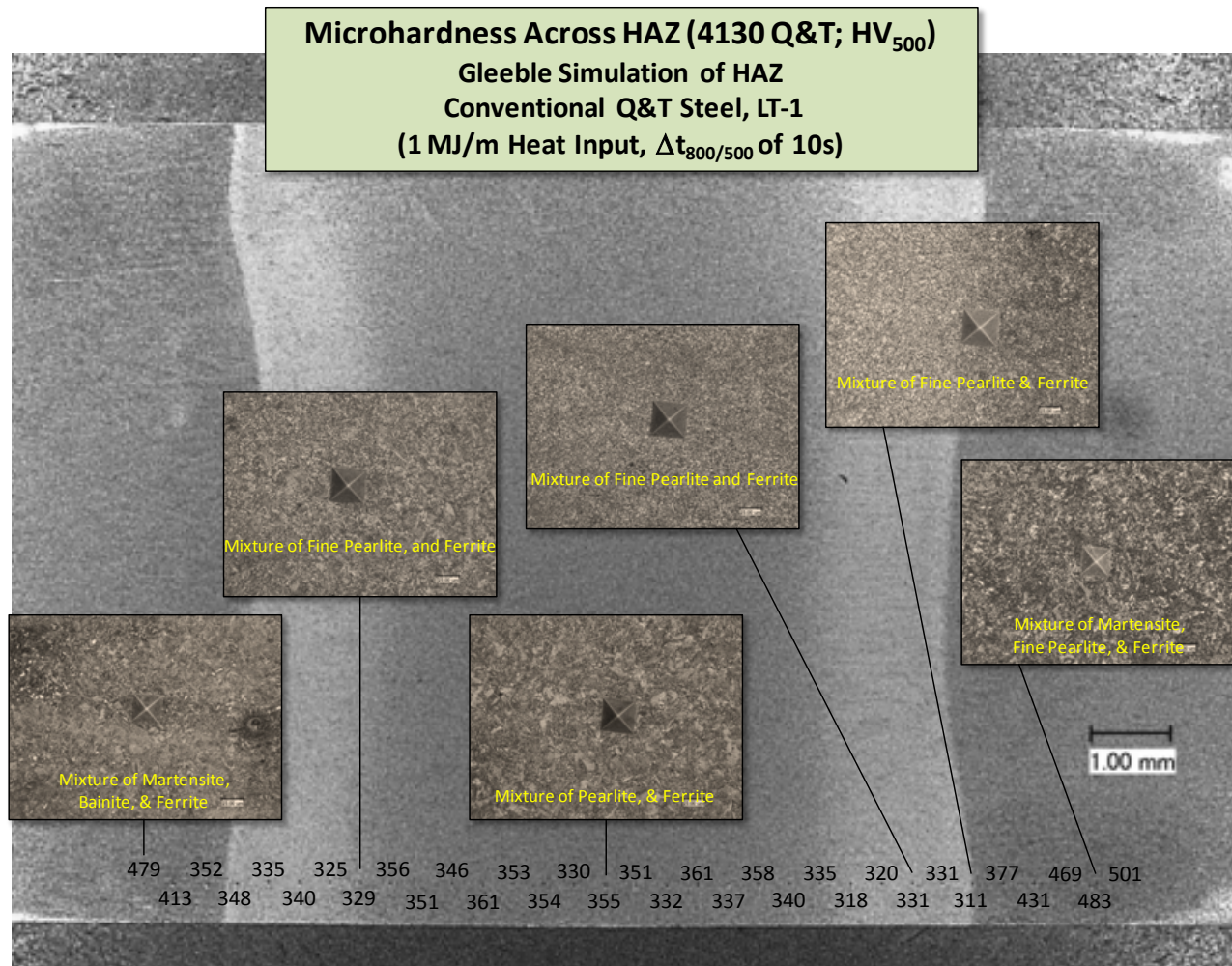


Figure 29. Photomicrographs and microhardness readings across the Gleeble HAZ in Q&T 4130 plate.

The CVN impact toughness is essentially the same for the FB and Q&T specimens tested after Gleeble HAZ processing. Results for the average impact energy for each condition can be found in Figure 30. The entire data is found in Appendix G. Figure 31 clearly shows that the predominant failure mode for the Gleeble processed CVN specimens was cleavage. This was not surprising considering the microstructure of the material (predominantly fine pearlite and ferrite).

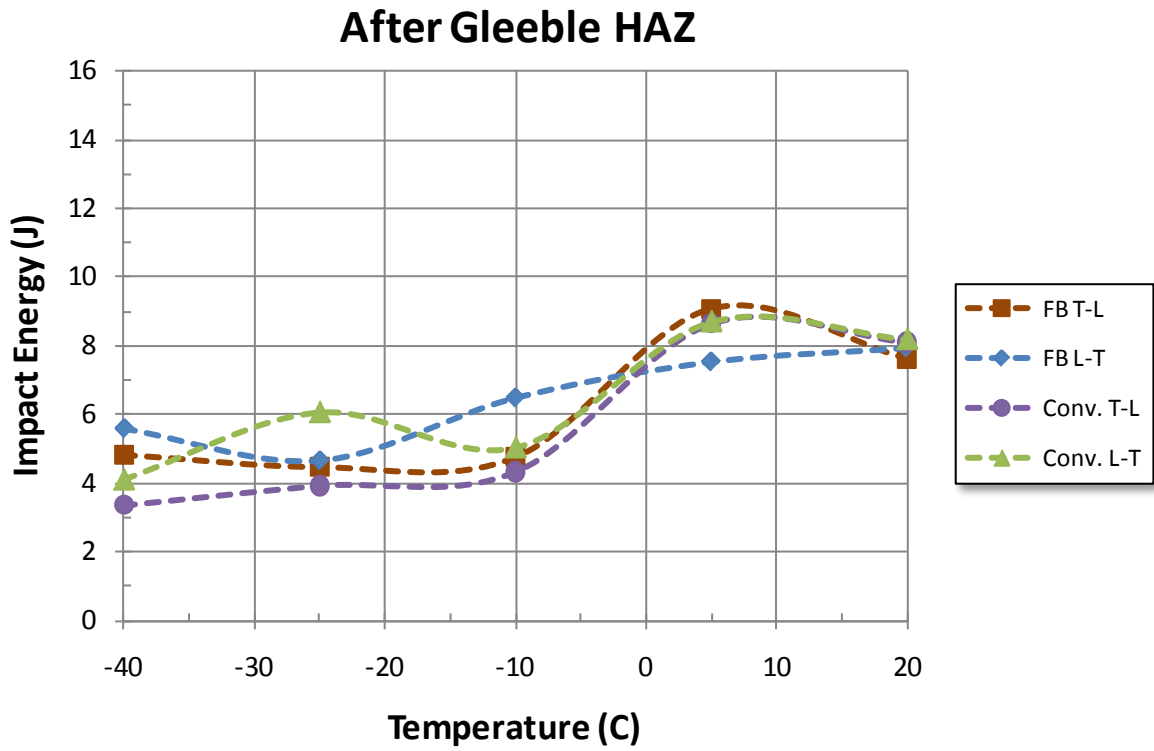
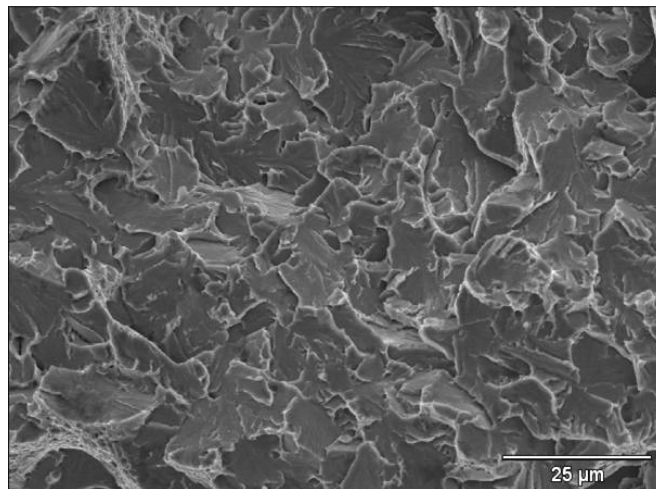


Figure 30. CVN impact toughness after Gleeble HAZ processing. Note the similarity in results between the FB and Q&T 4130 steel.



Figures 31. The predominant failure mode of the CVN Gleeble HAZ specimens was brittle cleavage fracture (the above specimen is C TL 04; 3.2J @ -40°C).

Applicability to Army and Other Applications

The major issues encountered during our testing were quench cracking of as-received FB plate and intergranular cracking in some FB CVN specimens. These issues need to be addressed prior to utilization of FB. Specific recommendations are made to address these issues and to further improve the quality, performance, and utilization of FB.

Though some issues were encountered, all-in-all, the performance of FB in our testing was positive and provided a good combination of mechanical properties. Moreover, the rapid processing of FB is more energy efficient and environmentally friendly than conventionally processed steel plate and other materials. As such, the costs to produce FB should be extremely reasonable and could enable widespread use for applications requiring very high strength and adequate elongation, ductility, and toughness. Current opportunities for flash bainite include armor and vehicle applications requiring ultra-high strength steels for high specific strength, weight reduction, and high cycle fatigue enhancement [17-20].

SUMMARY

- ARDEC performed testing and evaluation on 4130 steel plate that was flash bainite (FB) processed by Sirius Protection, LLC.
- Welding tests demonstrated that FB plate is weldable and that welded plate can subsequently be FB processed to restore strength. The loss of ductility might be attributable to lack of adequate weld process control (possible lack of penetration) or to something inherent in welded FB.
- All welded FB specimens passed bend testing. However, the results with ER120 filler metal were non-uniform, and demonstrated that the weak link was in the weld heat affected zone (HAZ).
- Tensile and fracture toughness testing of as-received FB exhibited an impressive mix of strength, elongation, ductility, and toughness.
- The welded FB plate contained relatively low tensile residual stress (+220 MPa), and the base FB material contained approximately 2% retained austenite. Any future work on thermal mechanical processing should attempt to produce compressive residual stresses.
- The impact toughness of the FB plate was consistently higher (~2x) than the Q&T plate at all test temperatures (20°C to -40°C). However, intergranular cracking was observed in half of the FB CVN specimens analyzed after testing. Additional testing is needed in order to determine if the source of the intergranular cracking is an insufficient temper,

and to determine if the intergranular cracking actually resulted in enhanced impact toughness due to off-axis, secondary cracking.

- The impact toughness testing on the Gleeble HAZ specimens from FB and Q&T material demonstrated equivalent results.

Though there are a few issues that need to be addressed, the FB processing of 4130 steel demonstrates promise for applications needing a combination of high strength with good elongation, ductility, and toughness (e.g. armor and vehicle). The novel FB process for steels has the potential to reduce product cost and weight while also enhancing mechanical performance.

RECOMMENDATIONS

- Eliminate edge cracking in FB plate and institute a non-destructive means to detect quench/edge cracking (e.g. magnetic particle inspection).

* Sirius Protection LLC has recently improved their heating process which results in more even heating of the steel plate. Purportedly, the last hundred 4130 steel plates have not experienced any edge cracking [21].

- Manage/Control S and P in 4130 plate in order to try to achieve enhanced toughness [20, 22].
- Fully evaluate the effects of thermal processing (austenitizing and tempering) on centerline intergranular cracking and toughness.
- If not already completed, perform formability, manufacturability (e.g. spot welding, paintability, etc.), fatigue, and delayed fracture (e.g. hydrogen embrittlement) studies relevant to the automotive industry.

ACKNOWLEDGEMENTS

The authors would like to acknowledge Gary Cola, Jr., Sirius Protection LLC, for providing 4130 plate material for testing and analysis, Jeffrey Schutz, ARDEC, for welding advice and guidance, Joe Indano, ARDEC, for welding, Emerson Childs, Benét Labs, for CVN testing, Chris Rickard, Benét Labs, for metallographic consultation, and Jonathan Montgomery for welding guidance and general consultation. The authors would also like to thank Barbara Machak and Alice Crayon for providing funding to support this effort.

REFERENCES

- [1] G.M. Cola, Jr., "Rapid Energy Efficient Production of Nano-Structured High Strength Metallic Structure and Armor with 0.30-cal APM2 M ϵ of 1.75 over RHA", 2010 DARPA Armor Challenge Report, 15 March 2010.
- [2] Y. Tomita and J. Okabayashi, "Mechanical Properties of 0.40 Pct C-Ni-Cr-Mo High Strength Steel Having a Mixed Microstructure of Martensite and Bainite", *Met. Trans. A*, 16A, Jan. 1985, pp. 73-82.
- [3] J.A. Kapp, L. Meisel, J. Barranco, P.J. Cote, and R.N. Wright, "Unusually High Fracture Toughness of ASTM A723 Steel From a Mixed Martensite/Bainite Microstructure", ARDEC Technical Report, ARCCB-TR-90032, Benét Laboratories, Watervliet, NY, Nov. 1990.
- [4] A. Crayon, "Flash Bainite", Memorandum for RDAR-D (J. Lannon), Benét Laboratories, Watervliet, NY, 08 June 2010.
- [5] Kou, S., Welding Metallurgy, John Wiley and Sons, New York, 1987, p. 50.
- [6] G. Krauss, "Solidification, Segregation, and Banding in Carbon and Alloy Steels", *Metallurgical and Materials Transactions B*, Vol. 34B, December 2003, pp. 781-792.
- [7] Teleconference with G. Cola, Jr., Sirius Protection LLC, 15 July 2010.
- [8] Cullity, B.D., Elements of X-ray Diffraction, 2nd edition, p. 281 – 292.
- [9] C.H. Curll, "Subsize Charpy Correlation with Standard Charpy", Technical Report No. Wal-TR-112/95, Watertown Arsenal Technical Report, December 1959.
- [10] ASM Handbooks Online, Mechanical Testing and Evaluation, Volume 8, Charpy Impact Testing, ASM, 2011.
- [11] Atlas of Isotherm Transformation and Cooling Transformation Diagrams, American Society for Metals, Metal Park, OH, 1977, p. 152.
- [12] Higgins, R.A., *Engineering Metallurgy: Applied Physical Metallurgy*, 6th Ed., Edward Arnold, 1993, pp. 249-250.
- [13] G. Krauss, "Martensitic Microstructures in Heat Treated Steels for Critical Vehicle, Machine, and Power Transmission Systems, *Proceedings from the 17th International Federation for Heat Treatment and Surface Engineering Congress*, 2008, pp. 10-17.
- [14] W.E. Wood, "Effect of Heat Treatment on the Fracture Toughness of Low Alloy Steels", *Engineering Fracture Mechanics*, Vol. 7, 1975, pp. 219-234.
- [15] E.R. Parker and V.F. Zackay, "Microstructural Features Affecting Fracture Toughness of High Strength Steels", *Engineering Fracture Mechanics*, Vol. 7, 1975, pp. 371-375.
- [16] Email communication between J. Montgomery, Army Research Laboratory, Aberdeen, MD, and G. Vigilante, Benét Laboratories, Watervliet, NY, 07 Feb. 2011.
- [17] K. Yamazaki et al., "Recent Advances in Ultra-High Strength Sheet Steels for Automotive Structural Use", Nippon Steel Technical Report #64, January 1995, pp. 37-44.
- [18] R. Lagneborg, "New steels and steel applications for vehicles", *Materials and Design*, Vol. 12, No. 1, February 1991, pp. 3-14.

- [19] T. Demir et al., "Investigation on the ballistic impact behavior of various alloys against 7.62 mm armor piercing projectile", *Materials and Design*, Vol. 29, 2008, pp. 2009-2016.
- [20] C.J. Hu, P.Y. Lee, and J.S. Chen, "Ballistic Performance and Microstructure of Modified Rolled Homogeneous Armor Steel", *Journal of the Chinese Institute of Engineers*, Vol. 25, No. 1, 2002, pp. 99-107.
- [21] Email communication between G. Cola, Jr., Sirius Protection LLC, and G.N. Vigilante, Benét Laboratories, Watervliet, NY, 15 January 2011.
- [22] Krauss, G., "Tempering of Martensite", *Encyclopedia of Materials: Science and Technology*, Elsevier Science, pp. 9093-9097, 2001.

APPENDIX A

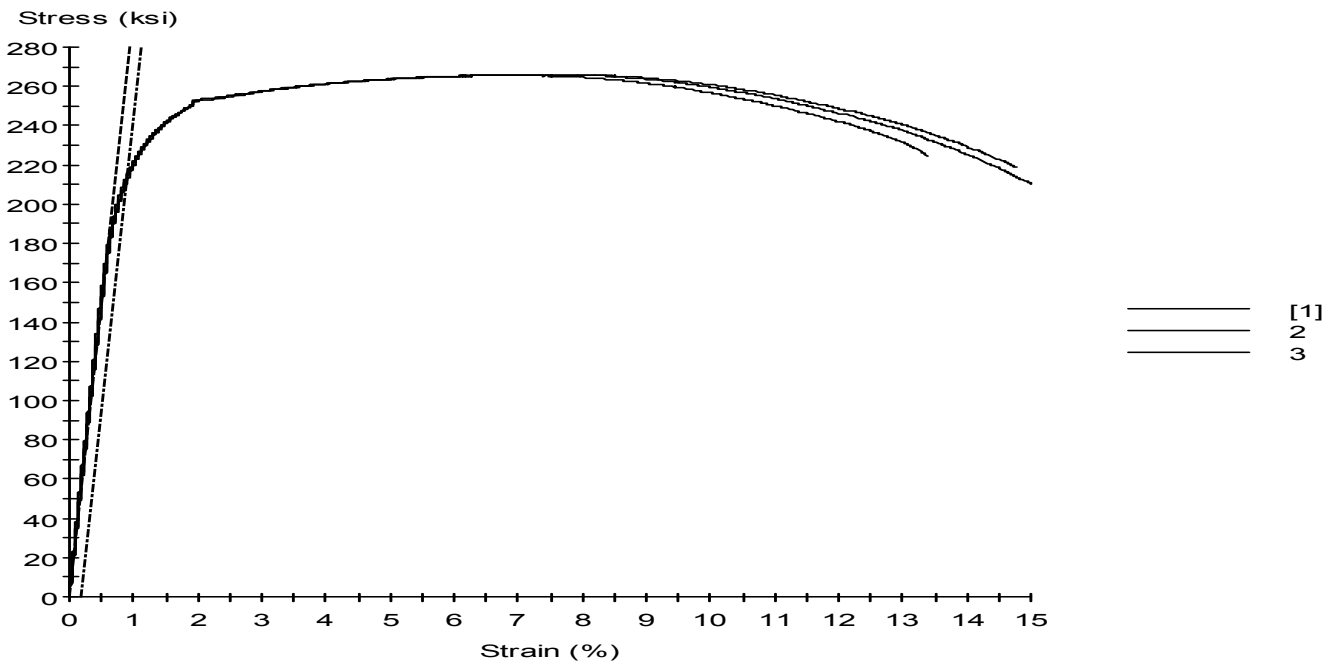
Tensile Test Results on "Baseline" FB Plate

Specimen Results:

Specimen #	Thickness mm	Final Thickness mm	Width mm	Final Width mm	Actual Gage Length mm	Measured Elongation mm	Failure Mode
1	6.147	4.775	6.325	4.892	25.215	29.058	Ductile
2	6.147	5.024	6.325	5.182	25.237	28.616	Ductile
3	6.147	4.826	6.325	4.953	25.258	28.992	Ductile
Mean	6.147	4.874	6.325	5.009	25.237	28.887	
Std. Dev.	0.000	0.132	0.000	0.152	0.023	0.239	

Specimen #	Hardness HRC	Area mm ²	Modulus GPa	Load At Offset Yield N	Stress At Offset Yield MPa	Peak Load N	Peak Stress MPa
1	50.5	38.877	207	57054	1468	71297	1834
2	51.2	38.877	215	56978	1466	71211	1832
3	51.0	38.877	208	57542	1480	71290	1834
Mean	50.9	38.877	210	57191	1471	71266	1833
Std. Dev.	0.4	0.000	5	306	8	48	1

Specimen #	Break Load N	Break Stress MPa	Calculated Percent Elongation %	Strain At Break %	Redux'n in Area %	Load Rate to Yield Mpa/min	
1	56426	1451	15.24	15.00	39.91	391	
2	60080	1546	13.39	13.38	33.04	374	
3	58618	1508	14.78	14.77	38.51	363	
Mean	58374	1502	14.47	14.38	37.15	376	
Std. Dev.	1840	48	0.97	0.88	3.63	14	



APPENDIX B

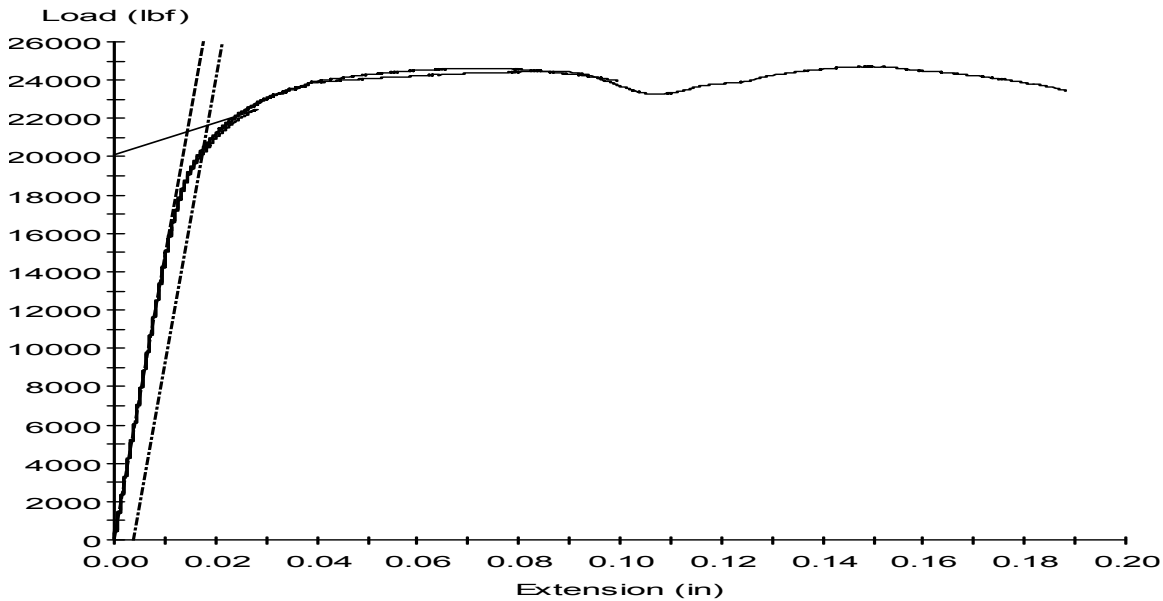
Tensile Test Results on Welded, Flattened and FB Plate

Specimen Results:

Specimen #	Failure Mode	Hardness Rockwell C	Actual Gage Length mm	Measured Elongation mm	Thickness mm	Thickness Reduced mm	Width mm
1	Brittle, angled	50.0	50.98	52.25	4.91	4.85	12.69
2	Ductile, angled	50.0	51.05	54.18	4.91	4.62	12.70
3	Ductile, angled	50.0	51.00	53.85	4.91	4.50	12.70
Mean		50.0	51.01	53.42	4.91	4.66	12.70
Std. Dev.		0.0	0.04	1.03	0.01	0.18	0.01

Specimen #	Width Reduced mm	Area mm ²	Modulus GPa	Load At Offset Yield N	Stress At Offset Yield MPa	Peak Load N	Peak Stress MPa
1	12.52	62.37	210	89,943	1,442	100,037	*
2	11.58	62.32	210	91,043	1,461	109,983	1765
3	11.68	62.32	211	91,474	1,468	109,531	1758
Mean	11.93	62.34	211	90,820	1,457	106,517	1761
Std. Dev.	0.52	0.03	0	790	13	5,617	5

Specimen #	Calculated Percent Elongation %	Strain At Break %	Area Redxn %	Load Rate To Offset Yield MPa/min	Break Load N	Break Stress MPa	
1	*	*	*	-	100,037	1604	Test error, slipped in grips.
2	6.12	*	14.11	748,569	108,474	1741	Slipped in grips.
3	5.58	4.92	15.71	808,011	106,747	1713	
Mean	5.85	4.92	14.91	778,294	105,086	1686	
Std. Dev.	0.38	0	1.13	42,032	4,457	72	



Despite large grip area and 10,000 PSI grip pressure, the specimens' ground smooth surface slipped in grips. The grips on 3rd specimen were roughened with abrasive paper and did not slip.

APPENDIX C

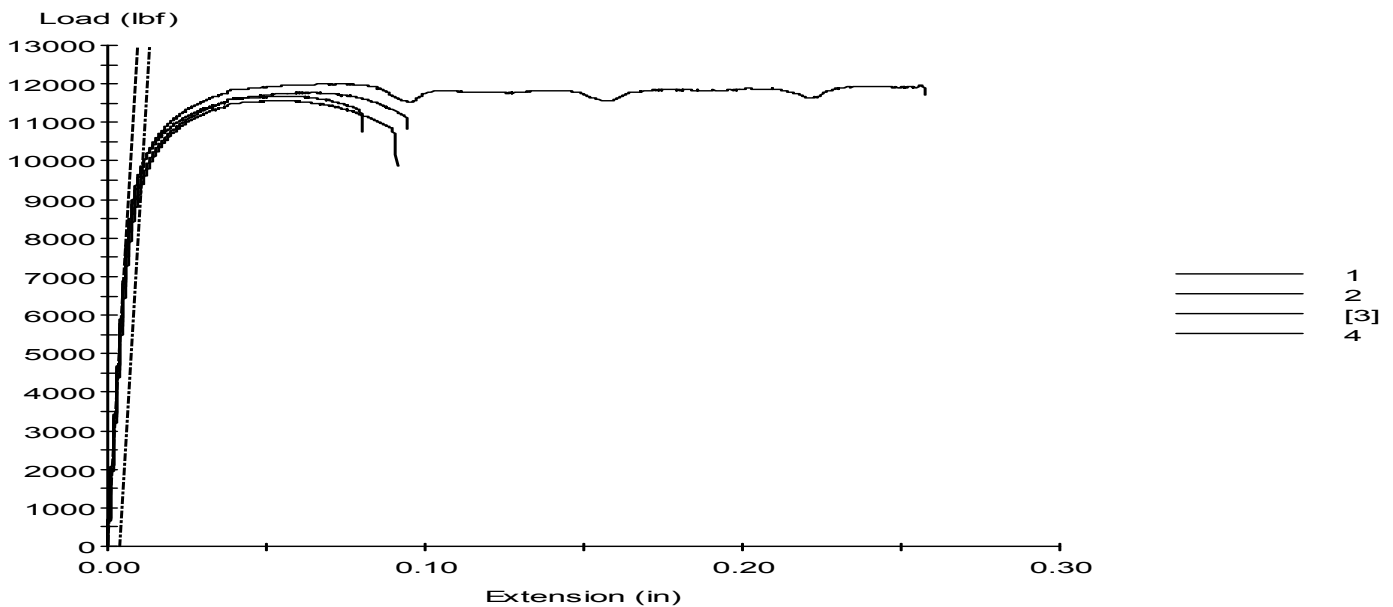
Tensile Test Results on FB Plate Welded with ER120 Filler Metal

Specimen Results:

Specimen #	Failure Mode	Hardness Rockwell C	Actual Gage Length mm	Measured Elongation mm	Thickness mm	Thickness Reduced mm	Width mm
1	Ductile	51.0	50.88	53.70	4.62	3.63	12.70
2	Ductile	51.0	50.88	53.24	4.62	3.63	12.70
3	Ductile	51.0	50.80	53.54	4.62	3.43	12.70
4	Ductile	51.0	50.71	53.04	4.62	3.73	12.70
Mean		51.0	50.82	53.38	4.62	3.61	12.70
Std. Dev.		0.0	0.08	0.30	0.00	0.13	0.00

Specimen #	Width Reduced mm	Area mm ²	Modulus GPa	Load At Offset Yield N	Stress At Offset Yield MPa	Peak Load N	Peak Stress MPa
1	11.10	58.71	194	42,365	722	51,435	876
2	11.20	58.71	212	44,040	750	51,970	885
3	11.07	58.71	202	42,778	729	52,392	892
4	11.43	58.71	207	44,134	752	53,381	909
Mean	11.20	58.71	204	43,329	738	52,295	891
Std. Dev.	0.16	0.00	8	892	15	824	14

Specimen #	Calculated Percent Elongation %	Strain At Break %	Area Redxn %	Load Rate To Offset Yield MPa/min	Break Load N	Break Stress MPa	
1	5.54	4.53	31.33	724,085	46,844	798	
2	4.64	4.01	30.70	698,939	49,507	843	
3	5.40	4.72	35.32	732,359	49,114	837	
4	4.59	*	27.31	705,917	52,874	901	Slipped in Grip
Mean	5.04	4.42	31.16	715,329	49,585	845	Some dbl necking.
Std. Dev.	0.50	0.37	3.29	15,534	2,487	42	



APPENDIX D

Representative K_{Ic} Fracture Toughness Result on "Baseline" FB Plate

Test Information						
Specimen ID		Bainite 2		Geometry		Bend
Contract		Bainite		Orientation		T-L
Material		4130 Flash Bainite		Yield (MPa)		1462.0
Temperature(C)		21.0		Tensile (MPa)		1793.0
Environment		40% RH		Modulus (GPa)		207.0
Specimen Dimensions						
Thickness (mm)		6.325		Notch Depth (mm)		3.683
Net Thickness (mm)		6.325		Gage Length (mm)		5.055
Width (mm)		12.500		Alpha Ratio		1.000
Height (mm)		50.800				
Precrack Parameters						
Pmax (N)		1334		Stress Ratio		0.100
Final a (mm)		6.408		Kmax (MPa sqrt (m))		20.28
Initial measured crack lengths (mm)						
6.2738	6.3754	6.477	6.3754	6.2992		
Test Results						
Crack Length (mm)		6.408		Pq (N)		4313
a/W		0.505		Pmax (N)		4585
				Kq (MPa sqrt (m))		65.54
Crack Strength Ratio		0.957		Kmax (MPa sqrt (m))		69.67
				Pmax/Pq		1.063
Validity Checks						
ASTM E399 Section		Requirement:			Status	Value
A2.3.3	$K_{precrack}/E \leq 0.002 \text{ in}^{1/2} (0.00032) \text{ m}^{1/2}$			valid	0.0006	
A2.3.3	$K_{precrack} \leq 60\% K_Q$			valid	18.46	
A2.4.1	Precrack stress ratio ≤ 0.1			valid	0.100	
7.3.2.2	Precrack length beyond notch $> 0.05\text{in} (1.27\text{mm})$			valid	0.102	
7.3.2.1	Precrack length between $0.45 < a/W < 0.55$			valid	0.505	
8.2.2	Straightness of 3 middle measurements			valid		
8.2.2	Additional criteria for chevron notch straightness			valid		
8.2.2	Minimum precrack length and surface measurement check			valid		
8.2.3	Crack plane must be within 10^0 of plane of symmetry			valid		
8.3	Load rate: 30 to 150 psi $\text{in}^{1/2}/\text{min} (0.55 \text{ to } 2.75 \text{ MPa m}^{1/2}/\text{sec})$			valid	60.04	
9.1.2	Ratio Pmax/PQ < 1.10			valid	1.063	
9.1.3	$2.5*(K_Q/\sigma_{ys})^2 < \text{then B and } a_{\text{average}}$			valid	0.198	

APPENDIX E
X-Ray Diffraction Report



...a member of the stresstech group of companies...

X-RAY DIFFRACTION SERVICE REPORT 3579

Residual Stress and Retained Austenite on a Welded Plate

Michael Hespos
US Army ARDEC
AMSRD-AAR-AEE-P
Bldg 60, M. Hespos
Picatinny Arsenal, NJ 07806

DATE COMPLETED: 20 January 2011

P.O. NO.: CC

DATE RECEIVED: 22 December 2010

SAMPLE ID & DESCRIPTION:

Residual stress measurements on a 4130 steel plate around an ER120 weld with a retained austenite measure on the bulk plate. Material properties are a Young's modulus of 205GPa and a Poisson's Ratio of 0.30.

MEASUREMENT TECHNIQUES IN COMPLIANCE WITH:

SAE 784a: Residual Stress Measurement by X-Ray Diffraction. Exception: AST uses a modern Modified-Psi diffractometer configuration instead of traditional Omega or Psi.

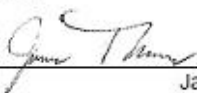
ASTM E915: Standard Test Method for Verifying the Alignment of X-Ray Diffraction Instrumentation for Residual Stress Measurement.

ASTM E975: Standard Practice for X-Ray Determination of Retained Austenite in Steel with Near Random Crystallographic Orientation.

Author-


Jonathan Mohan

Auditor-


James Thomas

American Stress Technologies, Inc.

www.astresstech.com

Address
840 Watercrest Way
Cheswick, Pa 15024
USA

Telephone
1 (724) 410 1030

Telefax
1 (724) 410 1031

E-mail
Info@astresstech.com

APPENDIX E

X-Ray Diffraction Report, Con't



Report 3579, Page 2 of 4
20 January 2011

Residual Stress Measurement Details

Radiation	CrK α , ~156°	Young's Modulus	205 GPa
Spot Size	Ø 3.5 mm	Poisson's Ratio	0.3
Tilt Settings (Psi)	-45° to 45°, 4/4	Power	30 kV, 9 mA
Oscillation	0°	Exposure Time	9s
Direction	0° (long), 45°, 90° (short)	Machine / Software. Ver.	X3000 G2R-1 / 1.22.10

Powder Check: 1/11/11 Avg -2.2 +/- 6.5 MPa, StDev 4.1

Retained Austenite Measurement Details

Radiation	CrK α , V Filtered	Oscillation	No
Exp. Time α -Fe / γ -Fe	80s / 800s	Power	30 kV / 9mA
Spot Size	Ø 3.5 mm	Tilt	45°
Sample Rotation	No	Machine / Software. Ver.	X3000 G2R-1 / 1.22.10

The sample was electropolished to a depth of greater than 150 μ m.

diffraction peak	α -Fe(211)	α -Fe(200)	γ -Fe(220)	γ -Fe(200)
	216.89	22.94	55.96	30.74

The R factors were calculated using ASTM E975; corrected for the modified Psi-geometry of the goniometer employed and the tilt angle of 45 degrees.

Results on reference samples were as follows:

1/18/11	2.44% reference, 1.9 +/- 0.2% (rotated)
1/18/11	14.9% reference, 14.3 +/- 0.8% (rotated)

American Stress Technologies, Inc.

www.astresstech.com

Address
840 Watercrest Way
Cheswick, Pa 15024
USA

Telephone
1 (724) 410 1030

Telefax
1 (724) 410 1031

E-mail
Info@astresstech.com

APPENDIX E

X-Ray Diffraction Report, Con't



Report 3579, Page 3 of 4
20 January 2011

Table 1: Results of residual stress and retained austenite measurements. Note the changes in peak width (fwhm) relative to location. The peaks collected for the retained austenite were disproportionate from what was expected causing the high deviation. This may be due to the presence of another phase such as carbide that overlaps the austenite 200 peak.

Top of Plate									
Direction	Left			Weld			Right		
	Stress [Mpa]	Dev [Mpa]	FWHM [Deg]	Stress [Mpa]	Dev [Mpa]	FWHM [Deg]	Stress [Mpa]	Dev [Mpa]	FWHM [Deg]
0	145	7.2	3.58	219	24.4	3.04	155	7.7	3.47
45	122	6.3	3.58	89	36.9	3.01	88	4.3	3.483
90	6	10.8	3.565	-16	40.8	2.885	78	8.6	3.497

Bottom of Plate									
Direction	Left			Weld			Right		
	Stress [Mpa]	Dev [Mpa]	FWHM [Deg]	Stress [Mpa]	Dev [Mpa]	FWHM [Deg]	Stress [Mpa]	Dev [Mpa]	FWHM [Deg]
0	124	10.5	5.43				32	10.8	5.26
45	133	16.3	5.41				-9	8.6	5.24
90	161	43.6	5.41				27	40.3	5.28

Bottom Plate			
Direction	Stress [Mpa]	Dev [Mpa]	FWHM [Deg]
0	209	5.5	4.73
45	131	7.7	4.72
90	104	35.4	4.70

Retained Austenite	
Austenite [%]	Dev [%]
2	1.4

APPENDIX E
X-Ray Diffraction Report, Con't



Report 3579, Page 4 of 4
 20 January 2011

Table 2: Calculated principal stresses. S1 is the maximum and S2 the minimum principal stresses, Sxy is the maximum possible shear stress and Theta is the rotation offset of the principal axis to the measurement axis.

Top of Plate				
		Left	Weld	Right
S1	[MPa]	159	219	164
S2	[MPa]	-8	-16	68
Sxy	[MPa]	84	118	48
Theta	[Deg]	17	-3	-18

Bottom of Plate				
		Left	Right	
S1	[MPa]	163	68	
S2	[MPa]	121	-9	
Sxy	[MPa]	21	38	
Theta	[Deg]	13	-43	

Bottom		
		Plate
S1	[MPa]	215
S2	[MPa]	98
Sxy	[MPa]	59
Theta	[Deg]	-13

APPENDIX F

Charpy V-Notch Test Results on Flash Bainite and Q&T 4130 Plate

Flash Bainite				
ID	Temp (°C)	Orientation	Impact Energy (J)	Ave (J)
FBL 32	-40	L-T	6.4	8.1
FBL 38	-40	L-T	8.7	
FBL 46	-40	L-T	9.2	
FBL 31	-25	L-T	6.5	7.7
FBL 40	-25	L-T	7.3	
FBL 48	-25	L-T	9.2	
FBL 33	-10	L-T	12.8	10.0
FBL 36	-10	L-T	8.5	
FBL 44	-10	L-T	8.7	
FBL 35	5	L-T	8.5	10.4
FBL 42	5	L-T	10.6	
FBL 50A	5	L-T	12.1	
FBL 34	20	L-T	10.1	11.5
FBL 43	20	L-T	11.1	
FBL 51	20	L-T	13.3	
FBT 33	-40	T-L	12.6	10.4
FBT 36	-40	T-L	9.2	
FBT 42	-40	T-L	9.5	
FBT 40	-25	T-L	7.1	7.9
FBT 48	-25	T-L	6.1	
FBT 51	-25	T-L	10.6	
FBT 30	-10	T-L	9.9	10.8
FBT 44	-10	T-L	14.1	
FBT 49	-10	T-L	8.3	
FBT 32	5	T-L	10.9	11.7
FBT 39	5	T-L	10.7	
FBT 46	5	T-L	13.6	
FBT 30A	20	T-L	15.6	15.2
FBT 34	20	T-L	15.1	
FBT 41	20	T-L	14.8	

Conventional Q&T				
ID	Temp (°C)	Orientation	Impact Energy (J)	Ave (J)
LT 2	-40	L-T	2.1	3.0
LT 8	-40	L-T	3.7	
LT 10	-40	L-T	3.2	
LT 1	-25	L-T	3.2	3.5
LT 11	-25	L-T	4.0	
LT 13	-25	L-T	3.2	
LT 7	-10	L-T	5.0	5.4
LT 14	-10	L-T	6.0	
LT 18	-10	L-T	5.1	
LT 9	5	L-T	5.6	5.6
LT 13	5	L-T	5.9	
LT 19	5	L-T	5.2	
LT 3	20	L-T	6.1	5.8
LT 6	20	L-T	5.8	
LT 12	20	L-T	5.5	
TL 5	-40	T-L	2.8	3.2
TL 18	-40	T-L	3.6	
TL 19	-40	T-L	3.1	
TL 3	-25	T-L	3.1	3.3
TL 6	-25	T-L	3.5	
TL 13	-25	T-L	3.2	
TL 4	-10	T-L	3.7	3.9
TL 6	-10	T-L	4.6	
TL 15	-10	T-L	3.5	
TL 1	5	T-L	3.8	3.6
TL 8	5	T-L	3.8	
TL 12	5	T-L	3.2	
TL 2	20	T-L	5.6	5.4
TL 14	20	T-L	5.7	
TL 17	20	T-L	5.1	

Flash Bainite - Mill Run				
ID	Temp (°C)	Orientation	Impact Energy (J)	Ave (J)
LT F3	-40	L-T	6.1	6.7
LT F4	-40	L-T	7.5	
LT F6	-40	L-T	6.4	
LT F1	20	L-T	16.3	15.6
LT F2	20	L-T	13.6	
LT F5	20	L-T	16.9	
TL F2	-40	T-L	6.6	6.1
TL F3	-40	T-L	6.7	
TL F6	-40	T-L	5.1	
TL F1	20	T-L	10.2	11.1
TL F4	20	T-L	11.9	
TL F5	20	T-L	11.1	

APPENDIX G

Charpy V-Notch Test Results on Gleeble HAZ Specimens

Flash Bainite					Conventional Q&T				
ID	Temp (°C)	Orientation	Impact Energy (J)	Ave (J)	ID	Temp (°C)	Orientation	Impact Energy (J)	Ave (J)
FB LT 9	-40	L-T	5.0	5.6	C LT 3	-40	L-T	4.1	4.1
FB LT 12	-40	L-T	5.8		C LT 12	-40	L-T	4.0	
FB LT 26	-40	L-T	6.0		C LT 20	-40	L-T	4.2	
FB LT 4	-25	L-T	4.4	4.7	C LT 5	-25	L-T	6.9	6.1
FB LT 16	-25	L-T	3.7		C LT 18	-25	L-T	6.0	
FB LT 24	-25	L-T	5.9		C LT 21	-25	L-T	5.3	
FB LT 5	-10	L-T	4.5	6.5	C LT 2	-10	L-T	6.4	5.0
FB LT 15	-10	L-T	5.7		C LT 15	-10	L-T	3.7	
FB LT 23	-10	L-T	9.3		C LT 17	-10	L-T	5.0	
FB LT 14	5	L-T	8.8	7.5	C LT 8	5	L-T	9.0	8.7
FB LT 18	5	L-T	7.1		C LT 11	5	L-T	7.1	
FB LT 22	5	L-T	6.7		C LT 16	5	L-T	9.9	
FB LT 11	20	L-T	7.4	8.0	C LT 7	20	L-T	8.0	8.2
FB LT 17	20	L-T	6.1		C LT 14	20	L-T	6.7	
FB LT 20	20	L-T	10.3		C LT 19	20	L-T	9.9	
FB TL 3	-40	T-L	5.4	4.8	C TL 4	-40	T-L	3.2	3.4
FB TL 10	-40	T-L	4.6		C TL 15	-40	T-L	3.2	
FB TL 12	-40	T-L	4.4		C TL 19	-40	T-L	3.6	
FB TL 1	-25	T-L	5.8	4.5	C TL 3	-25	T-L	4.1	3.9
FB TL 8A	-25	T-L	4.5		C TL 14	-25	T-L	3.7	
FB TL 13	-25	T-L	3.1		C TL 21	-25	T-L	3.9	
FB TL 11	-10	T-L	5.9	4.7	C TL 1	-10	T-L	5.2	4.3
FB TL 15	-10	T-L	3.9		C TL 6	-10	T-L	4.2	
FB TL 17	-10	T-L	4.4		C TL 20	-10	T-L	3.6	
FB TL 14	5	T-L	8.5	9.1	C TL 5	5	T-L	8.2	8.6
FB TL 19	5	T-L	9.9		C TL 9	5	T-L	10.0	
FB TL 20	5	T-L	8.8		C TL 13	5	T-L	7.8	
FB TL 7	20	T-L	9.2	7.6	C TL 2	20	T-L	9.5	8.1
FB TL 16	20	T-L	7.3		C TL 7	20	T-L	6.3	
FB TL 18	20	T-L	6.4		C TL 10	20	T-L	8.5	